



HAL
open science

Synthesis, NMR, Raman, thermal and nonlinear optical properties of dicationic ionic liquids from experimental and theoretical studies

Djebar Hadji, Boumediene Haddad, Silvia Antonia Brandán, Sumit Kumar Panja, Annalisa Paolone, Mokhtar Draï, Didier Villemin, Serge Bresson, Mustapha Rahmouni

► To cite this version:

Djebar Hadji, Boumediene Haddad, Silvia Antonia Brandán, Sumit Kumar Panja, Annalisa Paolone, et al.. Synthesis, NMR, Raman, thermal and nonlinear optical properties of dicationic ionic liquids from experimental and theoretical studies. *Journal of Molecular Structure*, 2020, 1220, pp.128713. 10.1016/j.molstruc.2020.128713 . hal-02880248

HAL Id: hal-02880248

<https://normandie-univ.hal.science/hal-02880248>

Submitted on 24 Jun 2020

HAL is a multi-disciplinary open access archive for the deposit and dissemination of scientific research documents, whether they are published or not. The documents may come from teaching and research institutions in France or abroad, or from public or private research centers.

L'archive ouverte pluridisciplinaire **HAL**, est destinée au dépôt et à la diffusion de documents scientifiques de niveau recherche, publiés ou non, émanant des établissements d'enseignement et de recherche français ou étrangers, des laboratoires publics ou privés.

Synthesis, NMR, Raman, thermal and nonlinear optical properties of dicationic ionic liquids from experimental and theoretical studies

Djebar Hadji ^a, Boumediene Haddad ^{a,b,*}, Silvia Antonia Brandán ^c, Sumit Kumar Panja ^d, Annalisa Paolone ^e, Mokhtar Draï ^f, Didier Villemin ^g, Serge Bresson ^h, Mustapha Rahmouni ⁱ

^a Department of chemistry, Dr. Moulay Tahar university of Saida, 20000 Saida, Algeria

^b Chemistry Laboratory of Synthesis, Properties, and Applications (CLSPA-Saida), 20000 Saida, Algeria

^c Cátedra de Química General, Instituto de Química Inorgánica, Facultad de Bioquímica. Química y Farmacia, Universidad Nacional de Tucumán, Ayacucho 471, (4000) San Miguel de Tucumán, Tucumán, Argentina.

^d Department of Chemistry, UkaTarsadia University, Maliba Campus, Gopal Vidyanagar, Bardoli, Mahuba Road, Surat-394350, Gujrat, India.

^e CNR-ISC, U.O.S. La Sapienza, Piazzale A. Moro 5, 00185 Roma, Italy

^f Université Djillali Liabes, BP 89, 22000 Sidi-Bel-Abbes, Algeria

^g LCMT, ENSICAEN, UMR 6507 CNRS, University of Caen, 6 bdMlJuin, 14050 Caen, France

^h Laboratoire de Physique des Systèmes Complexes, Université Picardie Jules Verne, 33 rue St Leu, 80039 Amiens cedex, France.

ⁱ Synthesis and Catalysis Laboratory LSCT, Tiaret University, Tiaret, Algeria

Abstract

In this work, two new di-cationic imidazolium based ILs containing chloride, (bisImCl) and hexafluorophosphate anion (bisImPF₆) have been synthesized and characterized by using FT-Raman and ¹H- and ¹³C-NMR spectroscopies. The p-xylyl group acts a spacer group between two imidazolium cations. B3LYP/6-311++G** calculations have optimized the structure of bisIm cation with both anion Cl in monodentate coordinations while in bisImPF₆ only a PF₆ group presents monodentate coordination. AIM calculations at the same level of theory have evidenced a higher number of interactions in bisImPF₆, as compared with bisImCl. The effect of anions on thermal properties has been investigated. The thermal behavior confirmed that bisImCl and bisImPF₆ have shown good thermal stability. The complete assignments for cation, bisImCl and bisImPF₆ are here reported together with a set of harmonic scaled force constants calculated for cation and bisImCl. Intermolecular and cation-anion interactions have been investigated by NMR spectroscopy. Further, polarizability (α) and the static first hyperpolarizabilities (β) of these ILs are calculated by DFT functionals in order to understand nonlinear optical (NLO) properties. It is also observed an inversed correlation between the predicted β value and the HOMO-LUMO energy difference ($\Delta\varepsilon$) from two state models. The high gap value observed for bisImPF₆ justify its low reactivity, as supported by high number interactions predicted for this ionic liquid.

Keywords: Dicationic Ionic liquids; Vibrational spectra; Coordination; NMR; Thermal study; Nonlinear optical properties.

* Corresponding author. Haddad boumediene

E-mail : E-mail: haddadboumediene@yahoo.com

1. Introduction

Ionic liquids (ILs) are fascinating ionic materials that have attracted considerable attention due to their unique properties, which can be tailored for specific applications ranging from chemical synthesis and separation processes to media for electrochemical devices [1–3]. Imidazolium-based ILs are very popular due to their chemical and thermal stability, well-established structural characterization, low viscosity, and their widespread potential applications [4,5]. For example, varying the substituents of the imidazolium ring drastically changes the physical properties of these ILs [6]. The attractive and potentially tunable properties of these fascinating materials make them not just replacements for conventional solvents, but open up opportunities to use them as new platforms for advanced multipurpose materials [7,8], for example by combining them with nanostructured materials [9]. Very recently, it has been pointed out that the chemical and physical properties of imidazolium-based ILs are determined by the interactions between the counter-ions. In addition, the ability to control and varying the substitutes of these ionic materials drastically changes the physical properties [10–12]. Further, studying DILs is another highly active area of research that aims at understanding the structure–property relationships. Despite the wealth of papers on DILs and their applications [13,14], there are a few experimental and computational studies on DILs to understand their structure-property relationships and NLO properties [15–17]. Studies of NLO properties of DILs are very important due to their potential applications in photonics and telecommunication, because each combination of anion and cation gives different value of NLO properties depending on the weak interaction of coupled cations with anions [16].

One of the major positive points in ionic compounds in the NLO behavior is the possibility of alignment of ionic chromophores, which can be controlled by changing the counter ion [17]. Moreover, such behavior depends on various parameters, such as the dispersion forces, the magnitude of interaction energy, and the hydrogen bonding interactions, the orientation and the predominant long-range coulombic forces [18]. From an experimental point of view, it is known, that the Z-scan technique is used to determine the NLO properties such as the nonlinear absorption and the index nonlinear refraction, due to its unpretentiousness [19]. It is also reported that change of the refractive index can induce variations of the heat conduction process, which is directly related to the nonlocal character of the optical nonlinearity [20]. Several theoretical studies [21–23] showed that large second-order NLO responses in ILs could increase the response time of electro-optic switching elements for optical information

processing and telecommunications. In order to determine the relation between NLO properties of ILs, Águila et al. [15] indicated that these ILs are good candidates for the development of NLO devices. Ostroverkhova et al. [24] showed that ILs can be used in materials for optical holographic recording, in catalysis [25] and for electrical-controlled memory systems [26]. It is possible to increase the NLO response of ILs, with the increase of the π -conjugation group and introduce strong anion. In our DILs, the opportunity to change the anion (Cl^- and PF_6^-) play a crucial role to increase the NLO response. To provide a more detailed understanding of the effect of chloride (Cl^-) and hexafluorophosphate (PF_6^-) anion in these two DILs (bisImCl and bisImPF₆) based with xylene spacer group on physical and electronic properties, TGA, NMR and Raman spectroscopic techniques are employed to characterize those two DILs. In addition, the NLO properties of two DILs (bisImCl and bisImPF₆) were analyzed by calculating their polarizability, anisotropy of polarizability and first hyperpolarizability by performing DFT calculation using different functionals.

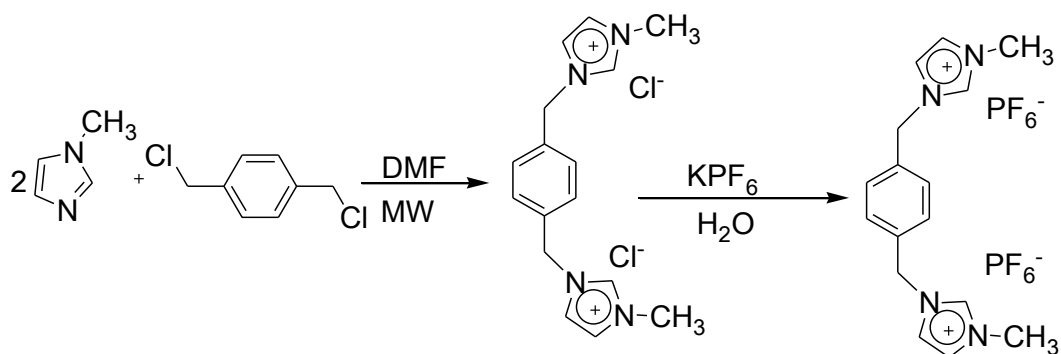
2. Materials and Methods

2.1.Synthesis and chemicals characterization

The reagents used in this study, 1-methyl-1H-imidazole (>99%), α,α' -dichloro-p-xylene (98%), diethyl ether and N,N-dimethylformamide, potassium hexafluorophosphate (99.5%) were purchased from Fluka and used as received. Deionized water was obtained with a Millipore ion-exchange resin deionizer.

2.1.1. Synthetic procedure of DILs:

BisImCl DIL is synthesized in the same ways as reported in our previous work [27]. As mentioned in the Scheme 1, the bisImCl DIL is dissolved in water and then an aqueous solution of KPF₆ is slowly added to the previous solution containing bisImCl DIL with constant stirring for 3 hrs at room temperature. After that, a white precipitate appeared from the resultant solution. The Dichloromethane (DCM) is added to the solution to dissolve the white precipitate. After that, DCM solution is washed with cold water at least 2-3 times. The presence of halide is checked by AgNO₃. Subsequently, DCM is dried with anhydrous MgSO₄. The DCM solution is further treated with activated charcoal to remove coloured impurities and then passed through a column containing alumina and celite. In order to remove volatile components and water, DIL are dried under constant stirring at a temperature of 298 K for 24 h at a reduced pressure of 2Pa. Finally, by means of a Metrohm 831, Karl Fischer titration is carried out to confirm the water content below 150 ppm.



Scheme 1. General synthesis of bisImCl and bisImPF₆ (MW = microwave)

After drying, the samples were handled under argon atmosphere. The yield of obtained bisImPF₆ was 76%. The structures of obtained DILs are confirmed by using ¹H, ¹³C, ¹⁹F, ³¹P-NMR and FTIR spectroscopy, in order to check the occurrence of the expected chemical reactions and confirm the absence of any impurities. The NMR analysis of both DILs is described in Section 3.3. Also, the ¹³C, ¹⁹F, ³¹P- NMR spectroscopic data are given in Supporting Information (Figure S1-S2).

2.2. Instrumentation

2.2.1. NMR Spectroscopy:

¹H-NMR (500 MHz), ¹³C-NMR (125.75 MHz), ¹⁹F-NMR (470.62 MHz) and ³¹P-NMR (202.47 MHz) spectra were recorded on a Bruker DRX 500 MHz spectrometer. Spectra were recorded in dimethylsulfoxide (DMSO-*d*₆), using the DMSO residual peak as the ¹H internal reference ($\delta = 2.5$ and 3.3), and the central peak of DMSO-*d*₆ at $\delta = 39.5$ for the ¹³C reference. Chemical shifts (δ) are given in ppm and referred to the internal solvent signal, namely TMS, H₃PO₄ and CFC₃, respectively.

3,3'-dimethyl-1,1'-(1,4-phenylenedimethylene)-bis(1H-imidazolium) dichloride

¹H-NMR (bisImCl) : (DMSO-*d*₆): δ_{H} (ppm) 9.48 (s, NCHN, 2H), 7.85 (s, NCHC, 2H), 7.74 (s, NCHC, 2H), 7.51 (s, -C₆H₄-, 4H), 5.47 (s, -CH₂-, 4H), 3.86 (s, 2×CH₃, 6H); ¹³C-NMR (DMSO-*d*₆):(δ ppm) 36.34, 51.67, 122.66, 124.62, 129.40, 135.73, 137.22.

FTIR (bisImCl) : ($\tilde{\nu}/\text{cm}^{-1}$): 3032 [$\nu(\text{C-H})_{\text{Arom}}$], 2874 [$\nu(\text{C-H})$], 1560 [$\nu(\text{C=C})$], 1442 [$\delta(\text{C-H})$], 1081 [$\nu(\text{C-N})$], 742 [$\nu(\text{C-H})$].

3,3'-dimethyl-1,1'-(1,4-phenylenedimethylene)-bis(1Himidazolium) bis(hexafluorophosphate)

¹H-NMR (bisImPF₆) : (DMSO-*d*₆): δ_{H} (ppm) 9.23 (s, NCHN, 2H), 7.74 (s, NCHC, 2H), 7.67 (s, NCHC, 2H), 7.47 (s, -C₆H₄-, 4H), 5.42 (s, -CH₂-, 4H), 3.84 (s, 2×CH₃, 6H); ¹³C-NMR (DMSO-*d*₆):(δ ppm) 36.25, 51.78, 122.68, 124.46, 129.42, 135.64, 136.95 ; ¹⁹F-NMR

(DMSO- d_6): δ_F (ppm)-70.7, -69.2 (d, J_{FP} = 711.25 Hz); $^{31}\text{P-NMR}$ (DMSO- d_6): δ_P (ppm) - 144.24, (septet, J_{PF} =711.58 Hz).

FTIR (bisImPF₆) (ν/cm^{-1}): 3174/3137[$\nu(\text{C-H})_{\text{Arom}}$], 2942 [$\nu(\text{C-H})$],1571[($\text{C}=\text{N}$)],1516 (C-C),1451[$\delta(\text{C-H})$], 1081 [$\nu(\text{C-N})$], 822 [$\nu(\text{P-F})$], 612 [$\nu(\text{C-H})$].

2.2.2. FT-IR and FT-Raman spectroscopy

Preliminary IR spectra were recorded on a FT-IR Perkin-Elmer Spectrum BX spectrophotometer with a resolution of 4 cm^{-1} in the range $4000\text{-}650\text{ cm}^{-1}$ in order to check the occurrence of the expected chemical reactions and the production of the DILs.

The FT-RAMAN spectra were acquired on a Vertex 70-RAM II Bruker FT-Raman spectrometer. This instrument is equipped with a Nd:YAG laser (yttrium aluminium garnet crystal doped with triply ionized neodymium) with a wavelength of 1064 nm and a maximum power of 1.5 W. The measurement accessory is pre-aligned: only the Z-axis of the scattered light is adjusted to set the sample in the appropriate position regarding the local measurement point. The RAM II spectrometer is equipped with a liquid nitrogen cooled Ge detector. FT-Raman spectra [$45\text{-}4000\text{ cm}^{-1}$] were collected with 1 cm^{-1} resolution by co-adding 128 scans for each spectrum at room temperature. The OPUS 6.0 software was used for the spectral acquisition, manipulation and transformation.

2.2.3. Thermal analysis

Concomitant thermogravimetric analysis (TGA) and differential thermal analysis (DTA) measurements were performed by means of a Setaram Setsys Evolution 1200 TG System. For each sample, a mass of $\sim 15\text{ mg}$ was used; the heating rate temperature was fixed at $5\text{ }^\circ\text{C}/\text{min}$ and the measurements were performed under a dynamical helium flux of $60\text{ ml}/\text{min}$.

2.2.4. Quantum Chemical Calculation

The DFT/B3LYP level having 6-311++G(d,p) basis set were employed to optimize the geometries of both DILs in gas phase. This level was also used for predicting the interactions between cation and anion in DILs by using the AIM 2000 program at the same level of theory [28,29]. Then, the scaled quantum mechanical force field (SQMFF) approach and the Molvib program were employed in the vibrational analysis together with the normal internal coordinates [30-32]. In the assignments process only those potential energy distribution (PED) contributions $\geq 10\%$ have been considered. The mean polarizability $\langle\alpha\rangle$, anisotropy polarizability $|\alpha|$, the hyper-Rayleigh scattering (HRS) first hyperpolarizability $\beta_{\text{HRS}}(-2\omega; \omega, \omega)$ and the depolarization ratio (DR) are reported and interpreted for these DILs. These calculations are performed using selected exchange-correlation (XC) DFT

functionals, B3LYP and CAM-B3LYP at the 6-311+G(d) and aug-cc-pVDZ basis sets. The Gaussian 09 suite of programs [33] was used for all calculations. The *GaussView* 5.1 program [34] was used to visualize the structures and the frontier molecular orbitals HOMOs and LUMOs. The dispersion effects were taken into account using the CAM-B3LYP functional with 6-311++G (d,p) basis set [35]. The Moldraw program was used to visualize the cations-anions interactions in both DILs and to calculate the volumes of cations and both DILs [36].

3. Results and discussion

3.1. Optimized structures of DILs

Optimized structures of BisIm cation, and ionic liquids BisImCl and BisImPF₆ in gas phase by using B3LYP/6-311++G** calculations can be easily seen in **Figure 1** while in **Figure 2** are shown the intermolecular cations-anions contacts by using the same level of theory with the Moldraw program [36]. R1 and R2 are designed to the five member's rings while R3 is named to six members ring. In BisImCl it is possible to observe monodentate coordinations of Cl atoms with C-H bonds of imidazolium groups while in bisImPF₆ only a PF₆ group is in monodentate coordination with the C-H bond corresponding to cation. This fact implies that the Cl atoms have higher facility to interaction with the H atoms of C-H bonds than the PF₆.

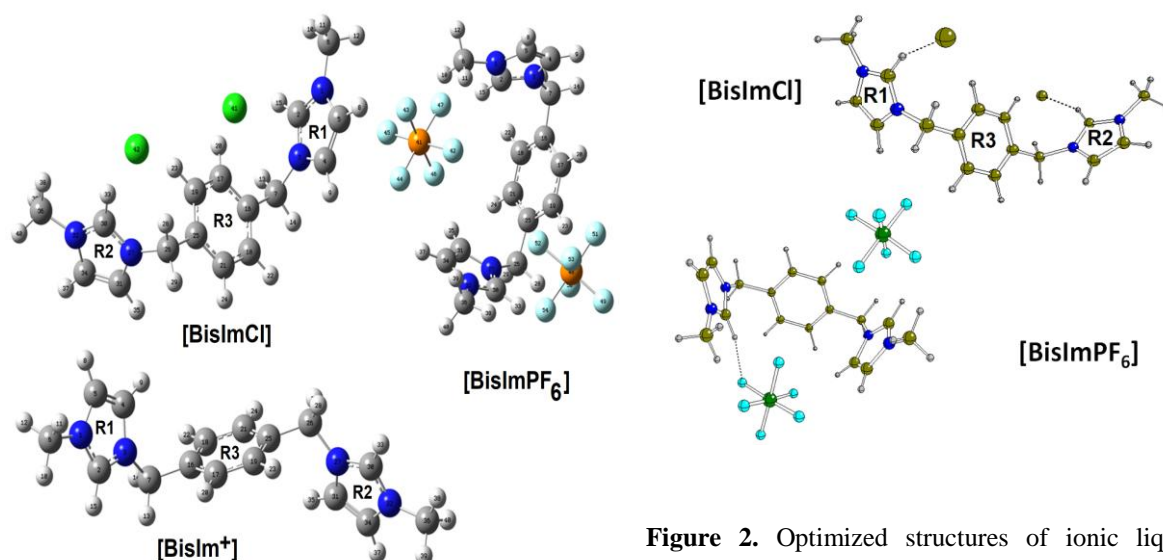


Figure 1. Optimized structures of bisIm cation, and ionic liquids bisImCl and bisImPF₆ in gas phase by using B3LYP/6-311++G** calculations.

Figure 2. Optimized structures of ionic liquids bisImCl and bisImPF₆ in gas phase showing the intermolecular cations-anions contacts by using B3LYP/6-311++G** calculations.

In **Table 1** are summarized calculated and corrected by ZPVE total energies, dipole moments and volumes of cation and ionic liquids bisImCl and bisImPF₆ in gas phase by using B3LYP/6-311++G** calculations. The ionic liquid bisImCl presents the higher dipole moment value probably due to great size of Cl atoms while the higher volume is observed for bisImPF₆. Note that the energies values have lower values when they are corrected by ZPVE, as also was observed in the ionic liquid 1-Ethyl-3-methylimidazolium hexafluorophosphate [37].

Table 1. Calculated and corrected by ZPVE total energies (*E*), dipole moments (μ) and volumes (*V*) of 3,3'-dimethyl-1,1'-(1,4-phenylenedimethylene)-bis(1H-imidazolium) cation [bisIm⁺] and ionic liquids 3,3'-dimethyl-1,1'-(1,4-phenylenedimethylene)-bis(1H-imidazolium) dichloride [bisImCl] and 3,3'-dimethyl-1,1'-(1,4-phenylenedimethylene)-bis(1H-imidazolium) bis(hexafluorophosphate) [bisImPF₆] by using B3LYP/6-311++G** calculations.

Species	E (Hartrees)	ZPVE (Hartrees)	μ (D)	<i>V</i> (Å ³)
B3LYP/6-311++G** Method				
[bisIm ⁺]	-840.4608	-840.1189	2.78	305.3
[bisImCl]	-1761.4232	-1761.0823	10.25	359.7
[bisImPF ₆]	-2722.5778	-2722.1967	8.91	470.0
Zero point vibrational energy (ZPVE)				

3.2. AIM studies

The Bader's theory is a tool very attractive to know the characteristics of different interactions by means of the topological properties by using the AIM 2000 program and the molecular graphics obtained accordingly [28,29]. For both bisImCl and bisImPF₆ the corresponding molecular graphics in gas phase by using B3LYP/6-311++G** calculations are given in **Figures 3 and 4**, respectively.

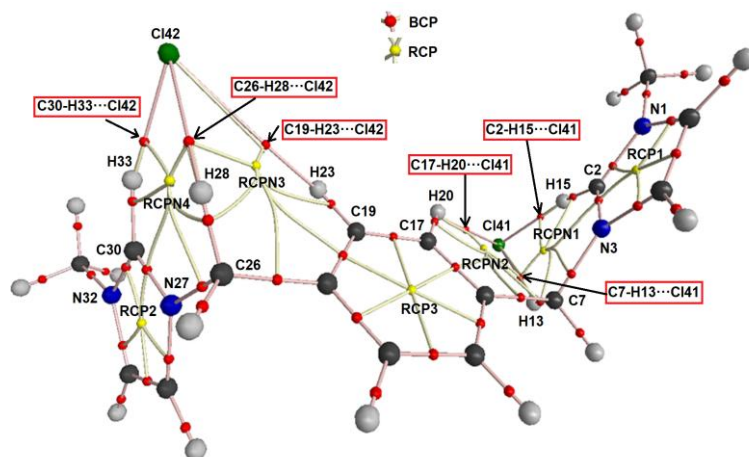


Figure 3. Molecular graphic of bisImCl in gas phase showing the intermolecular interactions by using B3LYP/6-311++G** calculations.

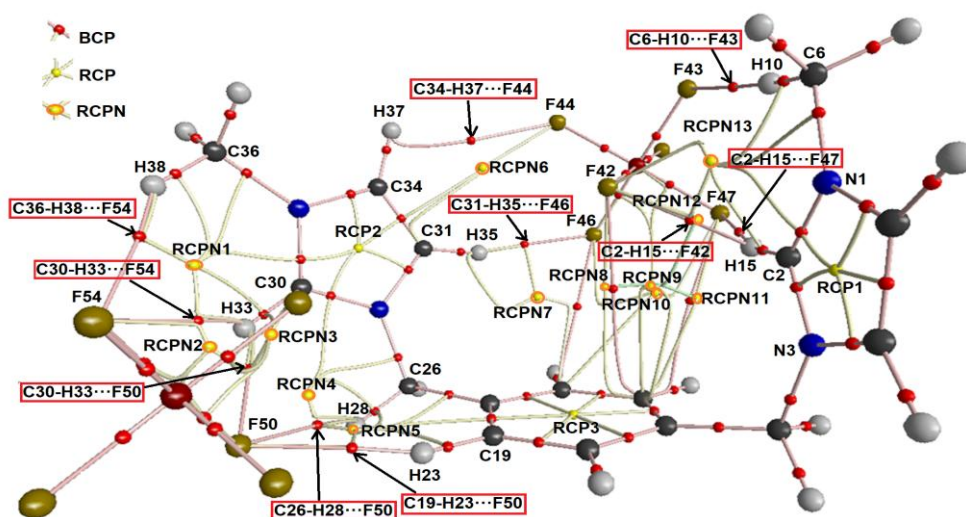


Figure 4. Molecular graphic of bisImPF₆ in gas phase showing the intermolecular interactions by using B3LYP/6-311++G** calculations.

Here, the topological properties are not presented due to the numerous interactions predicted for bisImPF₆. The ionic or highly polar covalent interactions with $\lambda_1/\lambda_3 < 1$ and $\nabla^2\rho(r) > 0$ (closed-shell interaction) are identified in the two figures (3-4) with red rectangles. RCPs of yellow colours are designed to the ring critical points while the BCPs of red colours are the bond critical points. The BCPs give rise to new critical points of rings called RCPN, where in bisImCl are observed four while in bisImPF₆ the number increase to thirteen. Six H bonds interactions are predicted in bisImCl which are: C2-H15...Cl41, C7-H13...Cl41, C17-H20...Cl41, C19-H23...Cl42, C26-H28...Cl42 and C30-H33...Cl42. The RCPs of the three rings are called RCP1, RCP2 and RCP3. Ten interactions are predicted for bisImPF₆ which

are C2-H15...F427, C2-H15...F47, C6-H10...F43, C34-H37...F44, C31-H35...F467, C19-H23...F50, C26-H28...F50, C30-H33...F50, C30-H33...F54 and C36-H38...F54. In this ionic liquid there are thirteen new RCPs. Hence, these studies suggest a high stability for bisImPF₆, as compared with bisImCl due to high number of H bonds interactions.

3.3. NMR Spectroscopy

The above studies have allowed observing that probably the different interactions in DILs and the nature of anion would significantly affect the ¹H-NMR chemical shifts when these ILs have strongly coordinating anions. For these reasons, the NMR spectroscopy has been widely used to elucidate the structure and cation-anion interactions in ILs [38-44].

For investigating intermolecular interactions and effect of anion on ¹H-NMR chemical shifts, bisImCl and bisImPF₆ DILs are chosen and presented in **figure 5**. From ¹H-NMR chemical shifts, six signals are obtained for each DILs. In the bisImCl, the characteristic peak for N-methyl protons (CH₃) appeared as a singlet at $\delta_H = 3.86$ ppm, the resonance of the methylene protons (-CH₂-) is observed as a singlet at $\delta_H = 5.47$ ppm. While, the aromatic phenyl groups (-C₆H₄-) resonates in the downfield region at $\delta_H = 7.51$ ppm, for the proton of imidazolium ring: C₄-H and C₅-H were displayed at $\delta_H = 7.74$ and 7.85 ppm, respectively. The chemical shift C₂-H was observed at 9.48 ppm for bisImCl and 9.23 ppm for bisImPF₆ DIL. As shown in **figure 5**, smaller differences in proton peaks are indeed within 0.02, 0.03, 0.04 ppm in $\delta_H(\text{CH}_3)$, $\delta_H(-\text{CH}_2-)$ and $\delta_H(-\text{C}_6\text{H}_4-)$ respectively, between bisImCl and bisImPF₆. The major difference observed with the protons in the imidazolium cation C₄-H and C₅-H, the peaks being shifted by 0.07, 0.11 ppm. The C₂-H proton shows that the difference in chemical shift is 0.25 ppm from bisImCl to bisImPF₆.

The ¹H-NMR spectra show more significant upfield shifts for bisImPF₆ compared to bisImCl. Moreover, these shifts are stronger for the aromatic protons (C₂-H, C₄-H/C₅-H) than for the methylene and phenyl ((CH₃), (-CH₂-), (-C₆H₄-)). The ¹H-NMR shift is largest for the C₂-H proton (from 9.48 ppm for bisImCl to 8.23 ppm for bisImPF₆ and slightly smaller for the C₄-H/C₅-H signals (from 7.85/7.74 ppm for bisImCl to 7.74/7.67 ppm for bisImPF₆). Headley et al.[39] have compared the ¹H and ¹³C-NMR spectra of 1-n-butyl-3-methylimidazoliumtetrafluoroborate (BMI⁺BF₄⁻) with that of 1-n-butyl-3-methylimidazoliumhexafluorophosphate (BMI⁺PF₆⁻) and found that the chemical shift of the H₂ proton in (BMI⁺BF₄⁻) moved significantly downfield compared to that of (BMI⁺PF₆⁻), suggesting that the anion plays a major role in determining the C₂-H chemical shift.

In our case, the finding clearly indicates that the chloride anion has the ability to form a tighter interaction with the hydrogen atoms C₂-H position of the imidazolium cation than PF₆, as observed in **figure 2**. On the other hand, the charge transfer between cations and anions plays a crucial role in the interionic interactions. Our results agree very well with previously published works [45,46]. It is also reported that the charge transfer in the case of the chloride anion is considerably higher than that of the hexafluorophosphate anion [47].

Chemical shifting towards upfield region values from chloride anion to PF₆, can be explained on basis of basicity nature and coordinating behaviour of anion. It is considered that PF₆ anion acts as one of the least basic anions, larger and weaker coordinating anion, supported by previous work [48,49].

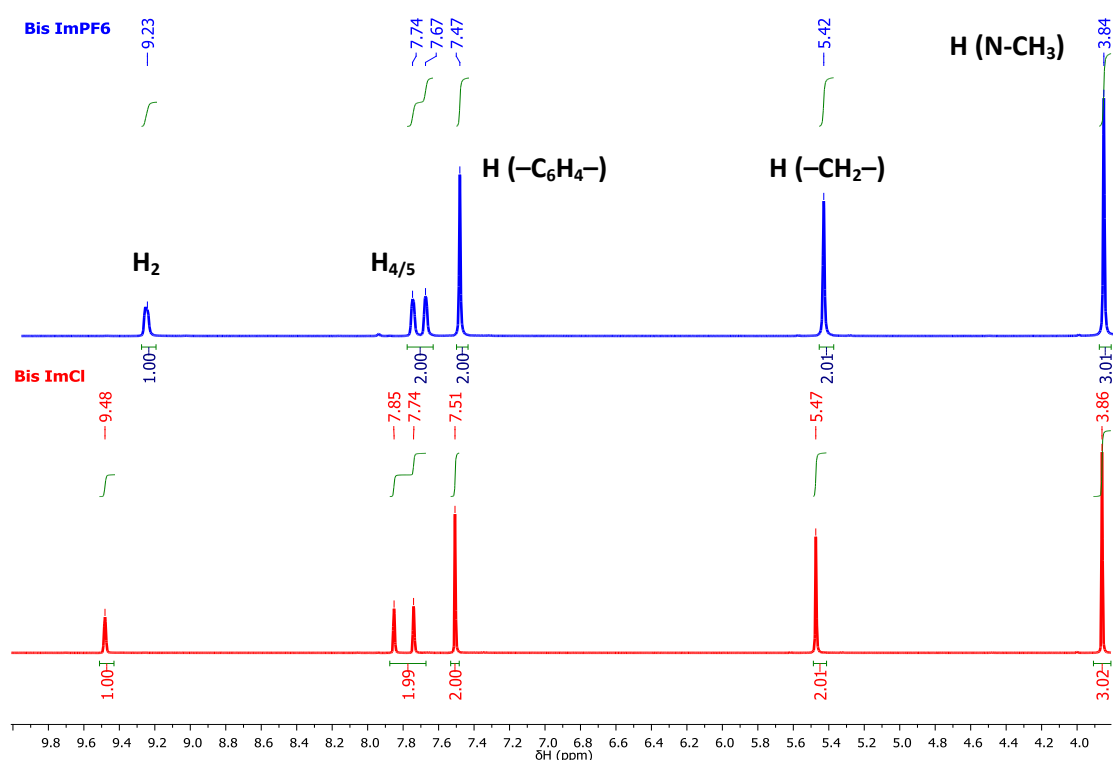


Figure 5. ¹H-NMR spectra of bisImCl and bisImPF₆ in DMSO-*d*₆.

The experimental ¹³C-NMR spectra of bisImCl and bisImPF₆ in DMSO-*d*₆ are presented in ESI-**FigureS1**. In ¹³C-NMR spectrum, seven signals were observed for both DILs. For the bisImCl, DIL, C₄ and C₅ carbons of imidazolium give signals and appeared at δ_c= 122.5, 124.4 ppm, respectively; while, the chemical shift of the C₂ signal is located at 137.2 ppm. In the other side, the aromatic phenyl carbons (-C_{aro}-) are highly electronegative and decrease the electron density at the ring carbon. Therefore, they show very high chemical shifts values observed at 129.40, 135.8 ppm. The peak for methylene (-C_{methylene}-) carbonis appeared at

51.5 ppm and the carbon of N-methyl (C_{methyl}) has peak at 36.2 ppm. Similarly, the ^{13}C -NMR signals of bisImPF₆ are approximately constant compared within the whole carbon groups in bisImCl and changes are very small. Both ^1H and ^{13}C -NMR results are in good agreement with those obtained from same analogues DILs with bromide anion published by Ibrahim et al. [45]. Finally, the ^{19}F of bisImPF₆ showed two signals at -70.8 and -69.3 ppm from coupling between six equivalent fluorine nuclei and phosphorus nucleus with coupling constant 711 Hz and septet (**Figure.S2**), both signals are very similar to those reported in our investigated meta -xylyl linked ionic liquids [49]. In case of ^{31}P -NMR spectrum, signal of P atom is appeared -144.3 ppm with coupling constant ($J_{\text{P-F}}$) 711.13 Hz [49]. Again, these values were found to be in good agreement with published data for related compounds [37, 54-55].

3.4. Vibrational study

B3LYP/6-311++G** calculations have optimized the structures of two DILs (bisImCl and bisImPF₆) and the corresponding to cation in gas phase with C_1 symmetries, for which, all modes are IR and Raman active. The number of vibrations modes expected for cation, bisImCl and bisImPF₆ are respectively 114, 120 and 154. Here, the SQMFF methodology, transferable scaling factors and normal internal coordinates were used together with the Molvib program to compute the harmonic force fields for cation and bisImCl while for bisImPF₆ only the bands predicted in the 4000-2000 cm^{-1} region due to the anharmonicity predicted were considered by using recommended scaling factors [30-32]. In **figure 6, 7 and 8** are presented the comparisons between the experimental Raman spectra in different wavenumbers regions. Our investigated DILs are composed of two cations bis-imidazolium linked with xylene spacer and two anions of chloride (Cl^-) and hexafluorophosphate (PF_6^-). The Raman spectra of both DILs were measured over the frequency range 45-4000 cm^{-1} . In **figures S3, S4 and S5** are presented comparisons between the predicted infrared and Raman spectra of cation, bisImCl and bisImPF₆. In **Table 2** are summarized observed and calculated wavenumbers (cm^{-1}) and assignments for cation and ionic liquids bisImCl and bisImPF₆ in gas phase by using B3LYP/6-311++G** calculations. The Raman spectra predicted in activities were converted to intensities. The detailed of the vibrational assignments are given below.

Table 2. Observed and calculated wavenumbers (cm^{-1}) and assignments for bisIm cation, and ionic liquids bisImCl and bisImPF₆ in gas phase by using B3LYP/6-311++G** calculations.

bisIm Cation			bisImCl		bisImPF ₆		
Ra ^a	SQM ^b	Assignment ^a	SQM ^b	Assignment ^a	Ra ^a	SQM ^b	Assignment ^a
3153	3158	vC31-H35	3156	vC31-H35	3180	3028	vC-H(R5)
	3158	vC4-H9	3156	vC4-H9	3163	3028	vC-H(R5)
3146	3140	vC30-H33	3138	vC34-H37	3143	3018	vC-H(R5)
	3140	vC2-H15	3138	vC5-H8	3118	3011	vC-H(R5)
	3138	vC34-H37	3042	vC17-H20	3084	3011	vC-H(R5)
3111	3138	vC5-H8	3035	vC18-H22	3074	2959	vC-H(R5)
3098	3052	vC18-H22	3031	vC19-H23	3069	2956	vC-H(R6)
3071	3049	vC19-H23	3027	v _a CH ₃ (C36)	3055	2929	vC-H(R6)
3067	3039	vC21-H24	3027	v _a CH ₃ (C6)	3051	2915	vC-H(R6)
3059	3036	vC17-H20	3018	vC21-H24	3046	2912	v _a CH ₃
3043	3036	v _a CH ₃ (C36)	3000	v _a CH ₃ (C36)	3041	2910	vC-H(R6)
3029	3036	v _a CH ₃ (C6)	3000	v _a CH ₃ (C6)	3030	2910	v _a CH ₃
3020	3023	v _a CH ₃ (C36)	2970	v _a CH ₂ (C26)	3023	2885	v _a CH ₃
3013	3023	v _a CH ₃ (C6)	2970	v _a CH ₂ (C7)	3007	2882	v _a CH ₂
3009	2992	v _a CH ₂ (C7)	2931	v _s CH ₃ (C36)	2989	2882	v _a CH ₂
2989	2992	v _a CH ₂ (C26)	2931	v _s CH ₃ (C6)	2981	2871	v _a CH ₂
2958	2947	v _s CH ₂ (C26)	2877	v _s CH ₂ (C7)	2976	2826	v _s CH ₂
2948	2947	v _s CH ₂ (C7)	2876	v _s CH ₂ (C26)	2965	2826	v _s CH ₂
2876	2944	v _s CH ₃ (C36)	2653	vC30-H33	2895	2814	v _s CH ₃
2817	2944	v _s CH ₃ (C6)	2602	vC2-H15	2844	2812	v _s CH ₃
						1656	vC=C(R6)
						1618	vC=C(R6)
						1610	vC=C(R5)
1615	1599	vC17-C19	1601	vC17-C19	1607	1607	vC=C(R5)
1583	1563	vC16-C18 vC21-C25 vC19-C25	1562	vC16-C18 vC21-C25	1585	1592	βC-H(R5)
1559	1553	vC4-C5	1548	vC4-C5	1563	1590	βC-H(R5)
1550	1553	vC31-C34	1548	vC31-C34	1557	1547	βC-H(R6)
1531	1531	vN3-C2	1530	vN27-C30	1522	1515	δ _a CH ₃
	1530	vN27-C30	1525	vN3-C2		1512	δ _a CH ₃
1468	1500	βC17-H20	1499	βC17-H20		1499	δ _a CH ₃
						1496	δ _a CH ₃
						1495	δCH ₂
						1490	δCH ₂
						1468	δ _s CH ₃
						1464	δ _s CH ₃
1452	1448	δ _a CH ₃ (C36)	1450	δ _a CH ₃ (C6)	1455	1459	βC-H(R6)
1446	1448	δ _a CH ₃ (C6)	1450	δ _a CH ₃ (C36)		1441	vC-N(A5)
1428	1433	δCH ₂ (C26) δCH ₂ (C7)	1432	δCH ₂ (C7) δCH ₂ (C26)	1431	1440	vC-N(A5)

1425	1430	$\delta\text{CH}_2(\text{C}7)$ $\delta\text{CH}_2(\text{C}26)$	1430	$\delta\text{CH}_2(\text{C}26)$	1418	1417	wagCH ₂
1418	1420	$\delta_a\text{CH}_3(\text{C}6)$	1428	$\delta_a\text{CH}_3(\text{C}36)$	1406	1402	ρCH_2
	1420	$\delta_s\text{CH}_3(\text{C}36)$	1428	$\delta_s\text{CH}_3(\text{C}6)$	1392	1379	wagCH ₂
1407	1411	vC18-C21 vC17-C19	1414	vC18-C21	1384	1374	ρCH_2
1404	1399	wagCH ₂ (C26) wagCH ₂ (C7)	1402	$\delta\text{CH}_2(\text{C}7)$	1377	1354	$\beta\text{C-H}(\text{A}6)$
1399	1399	$\delta_s\text{CH}_3(\text{C}36)$	1402	$\delta\text{CH}_2(\text{C}26)$ wagCH ₂ (C26)	1369	1343	$\beta\text{C-H}(\text{A}6)$
1389	1394	$\delta_s\text{CH}_3(\text{C}6)$	1394	$\delta_s\text{CH}_3(\text{C}6)$	1342	1341	vC-N
1385	1393	$\delta_s\text{CH}_3(\text{C}36)$ $\delta_s\text{CH}_3(\text{C}6)$	1394	$\delta_s\text{CH}_3(\text{C}36)$	1333	1332	vC-N
1359	1359	vN32-C30	1372	wagCH ₂ (C7)	1309	1313	$\beta\text{C-H}(\text{R}5)$
	1359	vN1-C2	1368	wagCH ₂ (C26)	1287	1307	$\beta\text{C-H}(\text{R}5)$
	1351	wagCH ₂ (C7) wagCH ₂ (C26)	1341	vN32-C34	1237	1231	$\beta\text{C-H}(\text{R}6)$
1340	1343	wagCH ₂ (C26) wagCH ₂ (C7)	1339	vN1-C5		1224	$\beta\text{C-H}(\text{R}6)$
1325	1315	$\beta\text{C}17\text{-H}20$ $\beta\text{C}19\text{-H}23$	1318	$\beta\text{C}18\text{-H}22$ $\beta\text{C}21\text{-H}24$	1218	1220	ρCH_2
1298	1298	vC21-C25	1306	vN32-C36	1211	1214	$\beta\text{C-H}(\text{R}6)$
1279	1281	vN32-C36	1297	vN1-C6		1212	$\beta\text{C-H}(\text{R}6)$
1279	1280	vN3-C4	1288	vC21-C25	1189	1176	$\beta\text{C-H}(\text{R}5)$
	1267	$\beta\text{C}2\text{-H}15$	1279	$\beta\text{C}30\text{-H}33$	1169	1174	$\beta\text{C-H}(\text{R}5)$
	1257	$\beta\text{C}2\text{-H}15$	1271	$\beta\text{C}2\text{-H}15$	1163	1158	ρCH_3
1215	1201	$\beta\text{R}_1(\text{A}3)\rho\text{CH}_2(\text{C}7)$	1213	$\rho\text{CH}_2(\text{C}7)$		1157	ρCH_3
1199	1194	$\beta\text{R}_1(\text{A}3)\rho\text{CH}_2(\text{C}7)$	1196	$\rho\text{CH}_2(\text{C}26)$	1147	1148	$\beta\text{C-H}(\text{R}6)$
1189	1188	$\rho\text{CH}_2(\text{C}26)$ $\rho\text{CH}_2(\text{C}7)$	1193	$\beta\text{R}_1(\text{A}3)$		1131	$\beta\text{C-H}(\text{R}5)$
1189	1183	$\beta\text{C}19\text{-H}23$ $\beta\text{C}17\text{-H}20$	1185	$\beta\text{C}17\text{-H}20$ $\beta\text{C}19\text{-H}23$	1122	1122	$\beta\text{C-H}(\text{R}5)$
1165	1171	vC26-C25	1172	vC26-C25	1111	1108	ρCH_3
1124	1131	$\beta\text{C}2\text{-H}15$	1145	vN27-C26	1102	1107	ρCH_3
	1131	$\beta\text{C}30\text{-H}33$	1143	vN3-C7	1043	1042	$\beta\text{R}_1(\text{R}5)$
1116	1117	$\rho'\text{CH}_3(\text{C}6)$	1123	$\rho'\text{CH}_3(\text{C}36)$	1036	1039	$\beta\text{R}_1(\text{R}5)$
1116	1117	$\rho'\text{CH}_3(\text{C}36)$	1123	$\rho'\text{CH}_3(\text{C}6)$	1036	1038	$\beta\text{R}_2(\text{R}5)$
1116	1110	vC18-C21	1108	vC18-C21 $\beta\text{C}21\text{-H}24$	1036	1037	$\beta\text{R}_1(\text{R}6)$
1092	1093	$\beta\text{C}34\text{-H}37\beta\text{C}5\text{-H}8$	1078	$\beta\text{C}4\text{-H}9\beta\text{C}5\text{-H}8$	1023	1034	$\beta\text{R}_2(\text{R}5)$
1092	1092	$\beta\text{C}4\text{-H}9\beta\text{C}31\text{-H}35$	1078	$\beta\text{C}31\text{-H}35\beta\text{C}34\text{-H}37$	1014	1014	$\gamma\text{C-H}(\text{R}6)$
1083	1068	$\rho\text{CH}_3(\text{C}6)$	1060	$\rho\text{CH}_3(\text{C}6)$ vN1-C2	988	973	$\gamma\text{C-H}(\text{R}6)$
	1068	$\rho\text{CH}_3(\text{C}36)$	1060	vN32-C30		967	$\gamma\text{C-H}(\text{R}6)$
1029	1017	$\beta\text{R}_1(\text{A}3)$	1021	$\beta\text{R}_1(\text{A}1)$	938	946	τwCH_2

1019	1017	$\beta R_1(A3)$	1020	$\beta R_1(A2)$	915	910	$\gamma C-H(R5)$
1019	1016	$\beta R_2(A1) \beta R_2(A2)$	1019	$\beta R_1(A3)$		900	$\gamma C-H(R5)$
1009	1006	$\nu N32-C34$	1012	$\gamma C17-H20$	888	889	$\gamma C-H(R5)$
1009	1006	$\nu N1-C5 \nu N27-C31$	993	$\nu N1-C5 \beta R_2(A1)$		882	$\gamma C-H(R5)$
989	987	$\gamma C18-H22$ $\gamma C21-H24$	992	$\nu N32-C34$ $\beta R_2(A2)$	865	859	$\gamma C-H(R6)$
951	977	$\gamma C19-H23$	971	$\gamma C30-H33$		856	$\gamma C-H(R5)$
882	896	$\tau wCH_2(C26)$ $\tau wCH_2(C7)$	968	$\gamma C2-H15$	843	850	$\nu_a PF_6$
860	874	$\gamma C34-H37$	952	$\gamma C21-H24 \gamma C18-H22$	836	845	$\nu_a PF_6$
860	874	$\gamma C5-H8$	909	$\tau wCH_2(C26)$	830	844	$\gamma C-H(R6)$
854	864	$\tau wCH_2(C26)$	877	$\tau wCH_2(C7)$	827	827	$\nu_a PF_6$
	860	$\gamma C18-H22$	869	$\gamma C19-H23$	815	817	$\nu_a PF_6$
848	846	$\gamma C17-H20$	844	$\gamma C31-H35 \gamma C4-H9$		814	$\nu_a PF_6$
839	835	$\gamma C2-H15$	841	$\gamma C4-H9$		813	$\gamma C-H(R6)$
832	821	$\gamma C2-H15$	836	$\gamma C21-H24 \gamma C18-H22$	806	809	$\nu_a PF_6$
810	819	$\gamma C30-H33$	827	$\nu C16-C17 \nu C19-C25$	769	760	$\gamma C-H(R5)$
780	767	$\tau R_1(A3)$	770	$\tau R_1(A3)$	741	758	$\gamma C-H(R5)$
772	765	$\nu C26-C25$ $\nu C7-C16$	761	$\delta N3C7C16$	738	739	$\gamma C-H(R5)$
767	745	$\gamma C4-H9$	725	$\gamma C34-H37$	720	736	$\gamma C-H(R6)$
767	745	$\gamma C31-H35$	724	$\gamma C5-H8$	702	709	$\tau R_1(R6)$
704	713	$\nu N27-C26 \nu N3-C7$	716	$\nu N27-C26 \nu N3-C7$	680	680	$\tau R_1(R5)$
656	686	$\tau R_1(A3)$	693	$\tau R_1(A3)$	672	679	$\tau R_1(R5)$
			656	$\nu N32-C36 \nu N1-C6$	667	675	$\nu_a PF_6$
641	648	$\beta R_2(A3)$	652	$\tau R_1(A3) \tau R_2(A1)$		655	$\tau R_2(R5)$
641	646	$\tau R_1(A3)$	645	$\beta R_2(A3)$	649	653	$\beta R_3(R6)$
641	641	$\nu N1-C6 \nu N32-C36$			643	639	$\tau R_2(R5)$
					629	633	$\nu N-C$
					621	625	$\nu N-C$
617	615	$\tau R_1(A2)$	612	$\tau R_1(A2)$	616	618	$\nu N-C$
611	615	$\tau R_1(A1)$	612	$\tau R_1(A1)$	572	568	$\nu C-C$
	603	$\tau R_2(A2)$	603	$\tau R_2(A1)$	548	535	$\nu_a PF_6$
587	600	$\tau R_2(A1)$	603	$\tau R_2(A2)$	548	532	$\nu_a PF_6$
544	556	$\beta R_3(A3)$	542	$\beta R_3(A3)$	532	528	$\delta_a FPF$
						527	$\delta_a FPF$
						526	$\delta_a FPF$
						526	$\delta_a FPF$
						525	$\delta_a FPF$
						524	$\delta_a FPF$
						522	$\delta_a FPF$
						515	$\nu_a PF_6$
510	496	$\tau R_3(A3) \tau R_2(A3)$	499	$\tau R_3(A3) \gamma C16-C7$ $\gamma C25-C26$	479	491	$\nu C-C$
					471	444	$\tau_w PF_6$

					469	443	$\tau_w\text{PF}_6$
					451	443	$\tau_w\text{PF}_6$
						442	$\tau_w\text{PF}_6$
						436	$\tau_w\text{PF}_6$
						436	δFPF
			417	$\beta\text{N1-C6}\beta\text{N3-C7}$	423	422	$\beta\text{N-CH}_3$
409	$\beta\text{N3-C7}$	408	$\beta\text{N32-C36}$			419	$\beta\text{N-CH}_3$
403	$\tau\text{R}_3(\text{A3})\tau\text{R}_2(\text{A3})$	402	$\tau\text{R}_2(\text{A3})$	409	408	τwCH_2	
391	$\beta\text{N1-C6}\beta\text{N32-C36}$	374	$\beta\text{C16-C7}\beta\text{C25-C26}$	385	389	$\tau\text{R}_1(\text{R6})$	
368	$\beta\text{C25-C26}$ $\beta\text{C16-C7}$	321	$\beta\text{C16-C7}$ $\beta\text{C25-C26}$	362	367	$\beta\text{R}_3(\text{R6})$	
311	$\gamma\text{C16-C7}\gamma\text{C25-C26}$	313	$\tau\text{R}_1(\text{A3})$	340	315	$\beta\text{C-C}$	
		303	$\tau\text{R}_2(\text{A3}) \tau\text{R}_3(\text{A3})$	298	297	ρFPF	
297	$\beta\text{C25-C26}$			296	296	ρFPF	
				291	292	ρFPF	
					290	ρFPF	
				282	285	wagFPF	
283	$\tau\text{R}_3(\text{A3})$				284	wagFPF	
					275	$\gamma\text{N-C}$	
252	$\gamma\text{N1-C6}\gamma\text{N32-C36}$	253	$\beta\text{N27-C26}$	268	268	$\gamma\text{N-C}$	
250	$\gamma\text{N32-C36}\gamma\text{N1-C6}$	250	$\gamma\text{N1-C6}\gamma\text{N3-C7}$	258	256	$\gamma\text{N-C}$	
204	$\gamma\text{N1-C6}\gamma\text{N32-C36}$	209	$\gamma\text{N32-C36}$		221	$\gamma\text{N-C}$	
194	$\beta\text{N3-C7}\beta\text{N27-C26}$	198	$\beta\text{N27-C26}\beta\text{C25-C26}$	211	210	$\gamma\text{N-CH}_3$	
166	$\gamma\text{N27-C26}\gamma\text{N3-C7}$	178	$\nu\text{H15-Cl41}$	183	189	$\gamma\text{N-CH}_3$	
141	$\tau\text{R}_3(\text{A3})\tau\text{R}_2(\text{A3})$	159	$\nu\text{H15-Cl41}\gamma\text{N1-C6}$		146	δNCC	
		130	$\gamma\text{N27-C26}$	133	130	τwCH_3	
					113	δNCC	
					107	δNCC	
		97	$\delta\text{C30H33Cl42}$		92	τwCH_3	
		82	$\tau\text{wCH}_3(\text{C6})$		76	$\tau\text{wC-N}$	
		81	$\tau\text{wCH}_3(\text{C36})$		75	$\tau\text{wC-N}$	
69	$\tau\text{wCH}_3(\text{C6})$	72	$\delta\text{C2H15Cl41}$		71	$\tau\text{wC-C}$	
69	$\tau\text{wCH}_3(\text{C36})$				61	$\delta\text{P-F}\cdots\text{H}$	
58	$\delta\text{N27C26C25}$ $\delta\text{N3C7C16}$	62	$\delta\text{C30H33Cl42}$ $\nu\text{H33-Cl42}$		59	$\delta\text{P-F}\cdots\text{H}$	
		53	$\tau\text{C2-H15}\tau\text{C30-H33}$		56	$\nu\text{C-H}\cdots\text{F}$	
		51	$\delta\text{N27C26C25}$		52	$\nu\text{C-H}\cdots\text{F}$	
					48	$\delta\text{C-H}\cdots\text{F}$	
40	$\tau\text{C25-C26}$	39	$\tau\text{C2-H15}$		43	$\tau\text{C-C}$	
		39	$\tau\text{C30-H33}$		36	$\tau\text{C-H}\cdots\text{F}$	
32	$\tau\text{C7-C16}$				32	$\tau\text{C-H}\cdots\text{F}$	
					26	$\tau\text{C-C}$	
25	$\tau\text{C26-N27}\tau\text{C7-N3}$	21	$\gamma\text{C16-C7}\gamma\text{C25-C26}$		25	τPF_6	
22	$\tau\text{C26-N27}\tau\text{C7-N3}$	18	$\tau\text{C7-N3}$		22	τPF_6	
14	$\tau\text{C25-C26}$	13	$\tau\text{C7-C16}\tau\text{C25-C26}$		15	$\tau\text{F}\cdots\text{H}$	
		12	$\tau\text{C26-N27}$		5	$\tau\text{F}\cdots\text{H}$	

Abbreviations: ν , stretching; wag, wagging; τ , torsion; ρ , rocking; τ_w , twisting; δ , deformation; a, antisymmetric; s, symmetric; a, antisymmetric; s, symmetric; (A₁), Ring 1; (A₂), Ring 2, (A₃), Ring 3.

^aThis work; ^bFrom scaled quantum mechanics force field B3LYP/6-311++G** method

C-H vibrations

Then C-H stretching modes are predicted by SQM calculations in the cation between 3158 and 3036 cm^{-1} while in bisImCl the C2-H15 and C30-H33 coordinated to the Cl atoms are predicted in the IR spectra intense at 2653 and 2603 cm^{-1} different from bisImPF₆ which are predicted at higher wavenumbers. In the Raman spectrum that C-H stretching mode in bisImCl is observed with lower intensity (**Figure S4**). As shown in **Figure 6**, the symmetric modes at 2817 and 2876 cm^{-1} in bisImCl and at 2844 and 2895 cm^{-1} for bisImPF₆ were assigned to the methyl group attached to the imidazolium rings N⁺-(CH₃) [27,47]. The bands at 2948, 2981, 2989 cm^{-1} for bisImCl and at 2965, 2981, 3007 cm^{-1} for bisImPF₆ corresponding to the methylene group (-CH₂-) [27]. While, the anti-symmetric modes of methyl group N⁺-(CH₃) attached to the imidazolium rings appeared at 3013, 3029, 3043 cm^{-1} for bisImCl and at 3023, 3046 cm^{-1} for bisImPF₆. Thus, the C-H stretching in imidazole ring are viewed experimentally by the presence of the bands from 3059 to 3153 cm^{-1} for bisImCl and from 3023 to 3180 cm^{-1} for bisImPF₆. The vibrational bands at lower wavenumbers can be referred to C(2)-H stretching modes, whereas those at higher wavenumbers can be assigned to the C(4,5)-H stretching modes [27, 46,49]. The detailed attributions of these bands for both investigated DILs are reported in **Table 2**. The C2-H15, C4-H9, C5-H8, C30-H33, C31-H35 and C34-H37 stretching vibrations corresponding to imidazole ring in cation, bisImCl and bisImPF₆ are predicted in expected regions [46,49]. On the other hand, the aromatic C17-H20, C18-H22, C19-H23 and C21-H24 modes of phenyl ring are predicted in the region of higher wavenumber for cation but for the two ionic liquids are predicted mixed among other stretching modes as observed in **Table 2**. The vibrational modes corresponding to two methyl groups (N-CH₃) are identified as (C6) and (C36) and

both are predicted in different regions in the three species and, hence, assigned as predicted by calculations.

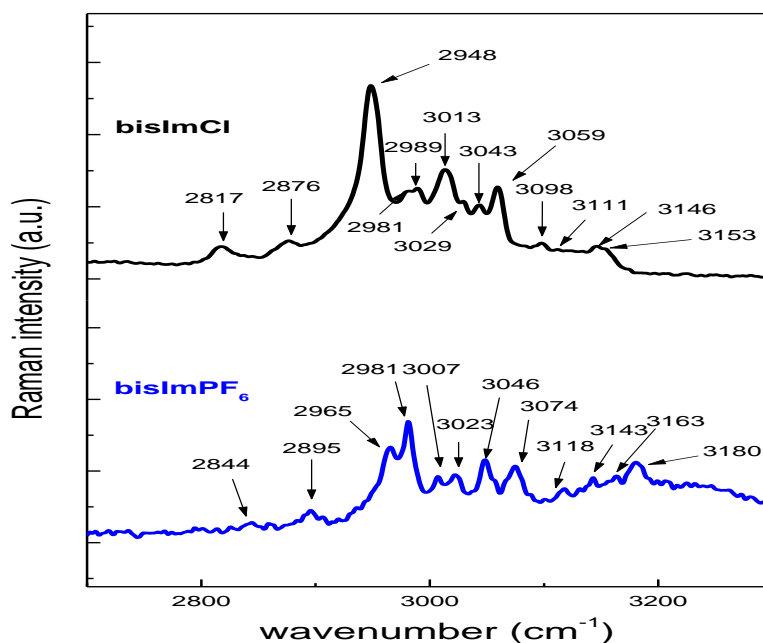


Figure 6. Experimental Raman vibrational spectra of bisImCl and bisImPF₆ in the frequency range 2600–3500 cm⁻¹.

C=C, C-C and C-N vibrations

The C=C vibrational frequencies are the significant characteristic bands in the vibrational spectra of phenyl and imidazolium rings, hence, the observed Raman bands at 1616, 1583, 1559 and 1550 cm⁻¹ are assigned to C=C vibrations for bisImCl, and at 1618 and 1607 cm⁻¹ in bisImPF₆ (**Figure 7**). This is in excellent agreement with the values predicted in our previous works [46,49].

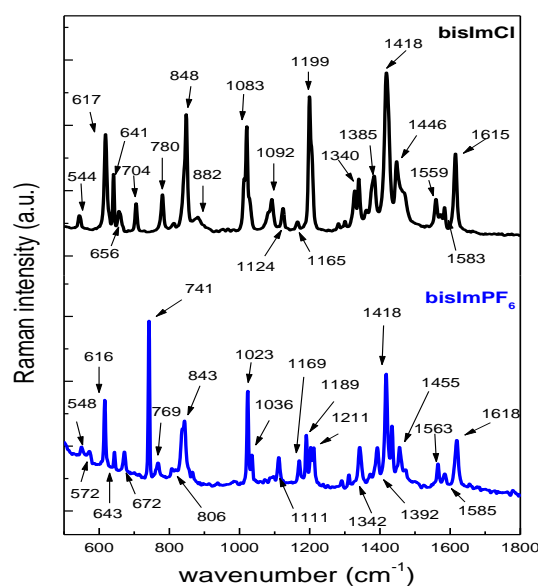


Figure 7. Experimental Raman vibrational spectra of bisImCl and bisImPF₆ in the frequency range 500–1800 cm⁻¹.

In the cation, the C–C, C–N stretching and in-plane N–C–H bending, related to the imidazole ring and the C–C aromatic stretching vibrations covering the spectral range from 1500 to 1110 cm⁻¹. The calculations predict the N–C stretching modes in the bisImCl at 1530, 1525, 1341, 1339, 1306, 1297, 1145 and 1143 cm⁻¹, hence, they can be assigned in these regions while in bisImPF₆ these modes are predicted at higher wavenumbers. Thus, these modes can be assigned to the Raman bands observed in those regions predicted by calculations. The C2–H15 and C30–H33 bending modes in the cation are predicted at 1267 and 1257 cm⁻¹ while the presence of Cl atoms in bisImCl produces a shifting of C2–H15 and C30–H33 bending modes toward higher wavenumbers. Hence, these two modes in the chlorinated ionic liquid are predicted at 1279 and 1271 cm⁻¹ while in bisImPF₆ both are predicted at 1176 and 1174 cm⁻¹. For these reasons, the Raman bands observed in these regions can be easily attributed to these vibration modes.

The SQM calculations predict the C–N stretching modes corresponding to N–CH₂ (N26–C26 and N3–C7) in bisImCl at 1145 and 1143 cm⁻¹ while in bisImPF₆ these modes are predicted at higher wavenumbers. Thus, those modes can be assigned accordingly and, as supported by literature data [52,53]. The C–C stretching vibrations of bisImCl are found at 1288, 1193, 1172 and 827 cm⁻¹ while in bisImPF₆ these modes are predicted in approximately the same regions but strongly mixed with bending modes of both five members rings and are in good agreement with those found in the characteristic group frequency tables [46,49].

PF₆⁻ anion vibrations

B3LYP/6-311++G** calculations have clearly predicted the vibrations modes of both PF₆ groups of bisImPF₆. The observed bands of the P–F stretching vibrations in bisImPF₆ DIL have been found to be very strong in the Raman spectra and these appear in the range 900–700 and 600–200 cm⁻¹ (**Figure 8**). The antisymmetric P-F stretching modes are assigned at 843 and 836 cm⁻¹ while the symmetric stretching mode is assigned to the Raman band at 806 cm⁻¹, as was observed in [EMIM⁺][PF₆⁻] [37]. The group of bands at 548 and 532 cm⁻¹ can be easily assigned to F-P-F deformations or scissors mode of PF₆ while the bands at 471, 469 and 451 cm⁻¹ are assigned to torsions of PF₆ anion. The bands at 298, 296 and 291 cm⁻¹ are assigned to rocking modes of these groups while the Raman band at 282 cm⁻¹ is assigned to wagging modes of these groups [37]. Assignments of the P–F stretching modes have been reported over the range by Talaty et al. [53].

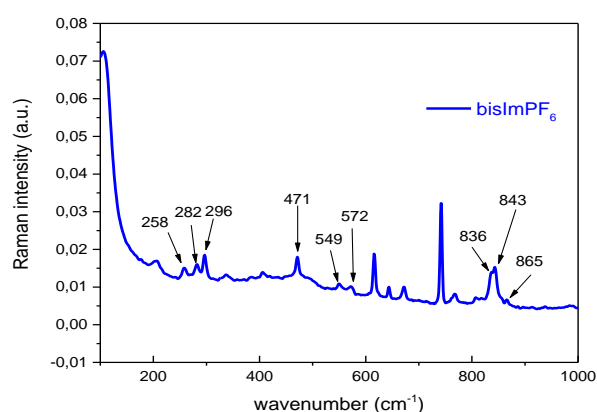


Figure 8. Experimental Raman vibrational spectra of bisImPF₆ in the frequency range 300–1000 cm⁻¹.

3.5. Force fields

Scaled internal force constants for [bisIm⁺] cation and ionic liquid [bisImCl] were calculated because these parameters are useful to predict the forces of different bonds. Thus, the harmonic force fields were used to compute those constants by using B3LYP/6-311++G** calculations. Comparisons of scaled internal force constants obtained for [bisIm⁺] cation and ionic liquid [bisImCl] in gas phase can be seen in **Table 3** compared with those reported for [EMIM⁺][PF₆⁻] [37]. The comparisons between the force constants for cation and [bisImCl] show that the incorporations of two Cl atoms to cation generate differences important in the

$f(\nu\text{C-H})_{R5}$ and $f(\nu\text{C=C})_{R5}$ force constants and affect slightly to $f(\nu\text{CH}_2)$ constants. Obviously, the Cl atoms due to its electronegativities are coordinated to cation by C-H...Cl bonds producing decreasing in the $f(\nu\text{C-H})_{R5}$ values while increase the values of $f(\nu\text{C=C})_{R5}$ force constants. Note that the cation-anion coordination is slightly higher in the ionic liquid [EMIM⁺][PF₆⁻] increasing the $f(\nu\text{C-H})_{R5}$ constant value to 5.41 mdyn Å⁻¹ and of the $f(\nu\text{C-N})_{R5}$ constant to 6.70 mdyn Å⁻¹ [37].

Table 3. Comparisons of scaled internal force constants for [bisIm⁺] cation and ionic liquid [bisImCl] in gas phase by using B3LYP/6-311++G** calculations.

Force constants	B3LYP/6-311++G**Method		
	[bisImCl] ^a	[bisIm ⁺] ^a	[EMIM ⁺][PF ₆ ⁻] ^b
$f(\nu\text{C-H})_{Hbond}$	5.04	5.08	5.45
$f(\nu\text{C-H})_{R5}$	4.97	5.39	5.41
$f(\nu\text{CH}_2)$	4.70	4.86	4.87
$f(\nu\text{CH}_3)$	4.92	4.96	4.89
$f(\nu\text{C-N})_{R5}$	6.53	6.57	6.70
$f(\nu\text{C-N})$	4.32	4.13	4.34
$f(\nu\text{C=C})_{R5}$	7.65	7.59	7.63
$f(\nu\text{C=C})_{R6}$	6.34	6.33	
$f(\delta\text{CH}_2)$	0.75	0.76	0.76
$f(\delta\text{CH}_3)$	0.55	0.54	0.54

Units are mdyn Å⁻¹ for stretching and mdyn Å rad⁻² for angle deformations

^aThis work, ^bFrom Ref [37].

3.6. Thermal properties

The thermal behavior of bisImCl and bisImPF₆ was investigated by means of concomitant TGA/DTA measurements. The experimental DTA data of bisImCl and bisImPF₆ DILs are shown in **figure 9**. Concerning the melting process, it was observed in bisImPF₆ by an endothermic peak at ~230°C, as result of a change from thermograms baseline. In the case of bisImCl, the DTA peak at the lowest temperature (~ 280 °C) seems to correspond to the first step of decomposition rather than to the melting process (see TGA results of figure 10).

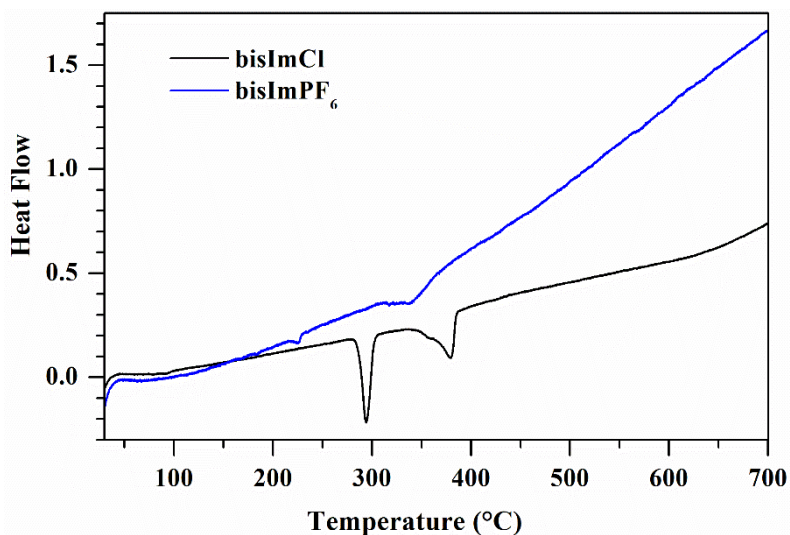


Figure 9. Heat flow (DTA) curves for the investigated bisImCl and bisImPF₆ DILs as a function of temperature.

Additionally, the TGA curve shows a multistep degradation process associated with the thermal decomposition of the PF₆ anion in the temperature range of 280–380 °C and the release next to bisIm cation in the temperature range 380–500 °C, respectively. The TGA study exactly fits and confirms the DTA study.

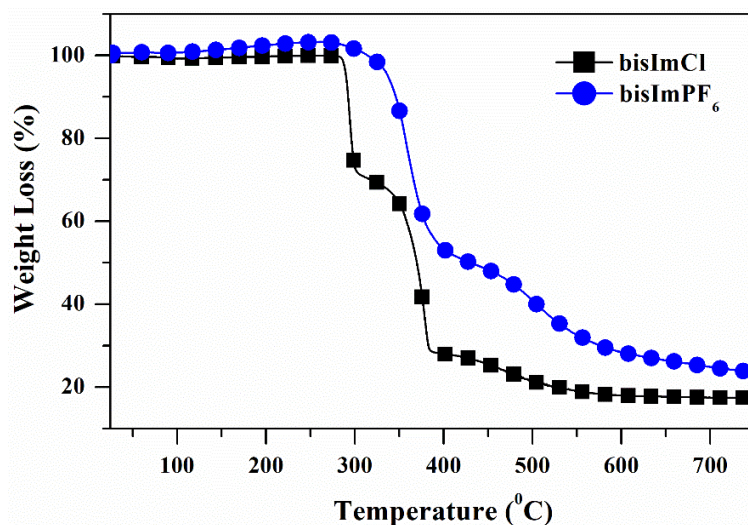


Figure 10. Thermal gravimetric analysis (TGA) for the investigated bisImCl and bisImPF₆ DILs.

From experimental results, it is clear that bisImCl and bisImPF₆ DILs are thermally stable at least up to 200°C and exhibit two different decomposition temperature values, which are included in the 280–400 °C range. The decomposition temperature of bisImCl is less than bisImPF₆ DIL. Nature of decomposition of bisimCl is different from bisImPF₆. From above

experimental results, it is clear that the anion can affect significantly on decomposition of these DILs and can be explained on basis of intermolecular interaction and coordinating nature of anion. Due to highly coordinating nature of PF₆ anion, the decomposition temperature of bisImPF₆ is higher than bisImCl DIL.

3.7. Electrical properties

The HRS first hyperpolarizability (β_{HRS}) can be deduced from electric field-induced second harmonic generation (EFISHG) measurements. Here, the β_{HRS} is related to the HRS intensity for non-polarized incident light and observation of plane-polarized scattered light made perpendicularly to the propagation plane. By using the HRS method, we can obtain several independent tensors for β calculation, which is not possible by EFISHG [56]. In HRS, the depolarization ratios (DR) can also be calculated. For a non-polarized incident signal, and for the reason that both polarizations are detected with equal sensitivity, the orientational average over β is:

$$\langle \beta_{\text{HRS}}^2 \rangle = \langle \beta_{\text{ZZZ}}^2 \rangle + \langle \beta_{\text{ZXX}}^2 \rangle \quad (1)$$

The full expressions of $\langle \beta_{\text{ZZZ}}^2 \rangle$ and $\langle \beta_{\text{ZXX}}^2 \rangle$ can be obtained from previously reported work [57]. The associated DR is defined as:

$$\text{DR} = \frac{I_{\text{VV}}^{2\omega}}{I_{\text{HV}}^{2\omega}} = \frac{\langle \beta_{\text{ZZZ}}^2 \rangle}{\langle \beta_{\text{ZXX}}^2 \rangle} \quad (2)$$

These two terms are orientational averages of the β_{ijk} tensor. All 10 calculated hyperpolarizability β_{ijk} contributions can be deduced from the direct hyperpolarizability calculations. These HRS invariants are calculated without assuming Kleinman's conditions.

$$\begin{aligned} \langle \beta_{\text{ZZZ}}^2 \rangle = & \frac{1}{7} \sum_{\zeta}^{x,y,z} \beta_{\zeta\zeta\zeta}^2 + \frac{4}{35} \sum_{\zeta \neq \eta}^{x,y,z} \beta_{\zeta\zeta\eta}^2 + \frac{2}{35} \sum_{\zeta \neq \eta}^{x,y,z} \beta_{\zeta\zeta\zeta} \beta_{\zeta\eta\eta} + \frac{4}{35} \sum_{\zeta \neq \eta}^{x,y,z} \beta_{\eta\zeta\zeta} \beta_{\zeta\zeta\eta} \\ & + \frac{4}{35} \sum_{\zeta \neq \eta}^{x,y,z} \beta_{\zeta\zeta\zeta} \beta_{\eta\eta\zeta} + \frac{1}{35} \sum_{\zeta \neq \eta}^{x,y,z} \beta_{\eta\zeta\zeta}^2 + \frac{4}{105} \sum_{\zeta \neq \eta \neq \epsilon}^{x,y,z} \beta_{\zeta\zeta\eta} \beta_{\eta\epsilon\epsilon} + \frac{1}{105} \sum_{\zeta \neq \eta \neq \epsilon}^{x,y,z} \beta_{\eta\zeta\zeta} \beta_{\eta\epsilon\epsilon} \\ & + \frac{4}{105} \sum_{\zeta \neq \eta \neq \epsilon}^{x,y,z} \beta_{\zeta\zeta\eta} \beta_{\epsilon\epsilon\eta} \\ & + \frac{2}{105} \sum_{\zeta \neq \eta \neq \epsilon}^{x,y,z} \beta_{\zeta\eta\epsilon}^2 + \frac{4}{105} \sum_{\zeta \neq \eta \neq \epsilon}^{x,y,z} \beta_{\zeta\eta\epsilon} \beta_{\eta\zeta\epsilon} \end{aligned} \quad (3)$$

$$\begin{aligned}
\langle \beta_{xzz}^2 \rangle = & \frac{1}{35} \sum_{\zeta}^{x,y,z} \beta_{\zeta\zeta\zeta}^2 + \frac{4}{105} \sum_{\zeta \neq \eta}^{x,y,z} \beta_{\zeta\zeta\zeta} \beta_{\zeta\eta\eta} - \frac{2}{35} \sum_{\zeta \neq \eta}^{x,y,z} \beta_{\zeta\zeta\zeta} \beta_{\eta\eta\zeta} + \frac{8}{105} \sum_{\zeta \neq \eta}^{x,y,z} \beta_{\zeta\zeta\eta}^2 \\
& + \frac{3}{35} \sum_{\zeta \neq \eta}^{x,y,z} \beta_{\zeta\eta\eta}^2 - \frac{2}{35} \sum_{\zeta \neq \eta}^{x,y,z} \beta_{\zeta\zeta\eta} \beta_{\eta\zeta\zeta} + \frac{1}{35} \sum_{\zeta \neq \eta}^{x,y,z} \beta_{\zeta\eta\eta} \beta_{\zeta\epsilon\epsilon} \\
& - \frac{2}{105} \sum_{\zeta \neq \eta \neq \epsilon}^{x,y,z} \beta_{\zeta\zeta\eta} \beta_{\eta\epsilon\epsilon} + \frac{2}{35} \sum_{\zeta \neq \eta \neq \epsilon}^{x,y,z} \beta_{\zeta\eta\epsilon}^2 - \frac{2}{105} \sum_{\zeta \neq \eta \neq \epsilon}^{x,y,z} \beta_{\zeta\eta\epsilon} \beta_{\eta\zeta\epsilon} \quad (4)
\end{aligned}$$

The B3LYP and CAM-B3LYP functionals were adopted for calculating the polarizability α , and first hyperpolarizability β , at the 6-311+G(d) and aug-cc-pVDZ basis sets. The results of the calculation after geometry optimization are reported in **Table 4**. Both DFT functionals showed high β_{HRS} values for both the bisImCl and bisImPF₆ DILs (**Table 4**). The results show in first the high values of the average polarizability $\langle \alpha \rangle$ obtained by the B3LYP and CAM-B3LYP functionals. The maximum value of $\langle \alpha \rangle$ in bisImPF₆ is 294.8 a.u. using CAM-B3LYP/6-311+G(d) calculation. Small differences in these values are obtained with different functionals and basis sets; however, the observed differences are insignificant. It must be noted that the average polarizability $\langle \alpha \rangle$ is mostly driven by the DILs size while the polarizability anisotropy $|\alpha|$ presents more subtle variations as a function of these DILs.

Table 4: B3LYP and CAM-B3LYP calculations of $\langle \alpha \rangle$, $|\alpha|$, β_{HRS} , DR in (a.u.) and $\Delta\epsilon$ in eV using 6-311+G(d) and aug-cc-pVDZ basis sets for bisImCl and bisImPF₆ DILs.

		bisImCl DIL				
		$\langle \alpha \rangle$	$ \alpha $	β_{HRS}	DR	$\Delta\epsilon$
B3LYP	6-311+G(d)	252.74	85.54	516.69	7.43	1.96
	aug-cc-pVDZ	266.34	90.33	474.55	7.49	1.99
CAM-B3LYP	6-311+G(d)	243.49	77.73	211.08	7.17	2.87
	aug-cc-pVDZ	257.59	82.98	183.77	7.15	2.94
		bisImPF ₆ DIL				
		$\langle \alpha \rangle$	$ \alpha $	β_{HRS}	DR	$\Delta\epsilon$
B3LYP	6-311+G(d)	249.88	36.77	145.76	7.57	3.19
	aug-cc-pVDZ	261.53	37.71	122.30	7.43	3.56
				115.70 ^a	7.10 ^a	
CAM-B3LYP	6-311+G(d)	294.80	34.24	127.74	7.51	3.37

aug-cc-pVDZ	257.04	35.34	105.95	7.35	4.01
-------------	--------	-------	--------	------	------

^aB3LYP/6-31+G(d,p) for similar IL[58]

DFT/B3LYP calculation gives the highest β_{HRS} values for bisImCl DIL, the CAM-B3LYP functional shows satisfactory hyperpolarizability results (**Table 4** and **Figure 12**). From our previous studies [59–61], it can be stated that the CAM-B3LYP functional has shown to predict reliable hyperpolarizability of different compounds. In case of the presence of the PF_6^- , and using the 6-311+G(d) and aug-cc-pVDZ basis sets, the B3LYP functional gives the lowest values of the mean polarizabilities (α). On the other hand, the bisImCl shows the highest β_{HRS} values ($\beta_{\text{HRS}} = 516.6$ a.u.) using the B3LYP/6-311+G(d) calculation. Shkir et al. [62] showed that the hyperpolarizability in ILs strongly depends on cation-anion interactions. In our ILs, the β_{HRS} of bisImCl is 474.5 a.u. and for the bisImPF₆, the β_{HRS} is 122.3 a.u. using B3LYP/aug-cc-pVDZ calculation. Therefore, the effect of the anion on the first hyperpolarizability values is crucial. This is maybe due to the stronger Coulombic interactions and the weaker van der Waals interactions in the case of bisImCl ion-pairs, whereas in the bisImPF₆ ion-pairs, the charge is more dispersed reported by Raabe et al. [63]. This interaction plays an important role to affect the NLO properties. The understanding of these interactions is a challenge in particular for ILs.

Bishop et al. [64] had compared first hyperpolarizabilities (β) of ions and showed that the chloride ion (Cl^-) had a strong first hyperpolarizability (β) compared to the ions studied in their paper. Also, the high hyperpolarizability of bisImCl can be related to the high binding energy between the Cl^- and the cation [65]. We can calculate this energy by doing the differences between the total energies of the ion pairs and the separated ions. Zhang et al. [66] showed that the binding energies are dependent dramatically on the second hyperpolarizability. On the other hand, Rodriguez et al. [58] showed in their study of the β_{HRS} in ILs using DFT calculations, that the presence of PF_6^- anion in their series of ILs reduces the β_{HRS} values compared to BF_4 and TFSI anions. Similar findings are observed in our present work. The β_{HRS} of each DILs studied in this work is affected by the cation-anion interaction, the cation-anion association results in electron charge redistribution, which characterise by a predominant dipolar nature. Indeed, the DR values show the dipole character for these DILs (**Table 4** and **Figure 11**), their values are range from 7.1 to 7.5 using CAM-B3LYP calculations. The HRS value of bisImPF₆ is obtained at the B3LYP functional is same to the PF_6^- anion-based imidazolium IL (bmimPF₆) [58]. The first hyperpolarizability β of these DILs

is more than five times higher than the urea [67,68] using B3LYP/aug-cc-pVDZ. From theoretical results, it can be stated that these DILs have shown very good NLO activity.

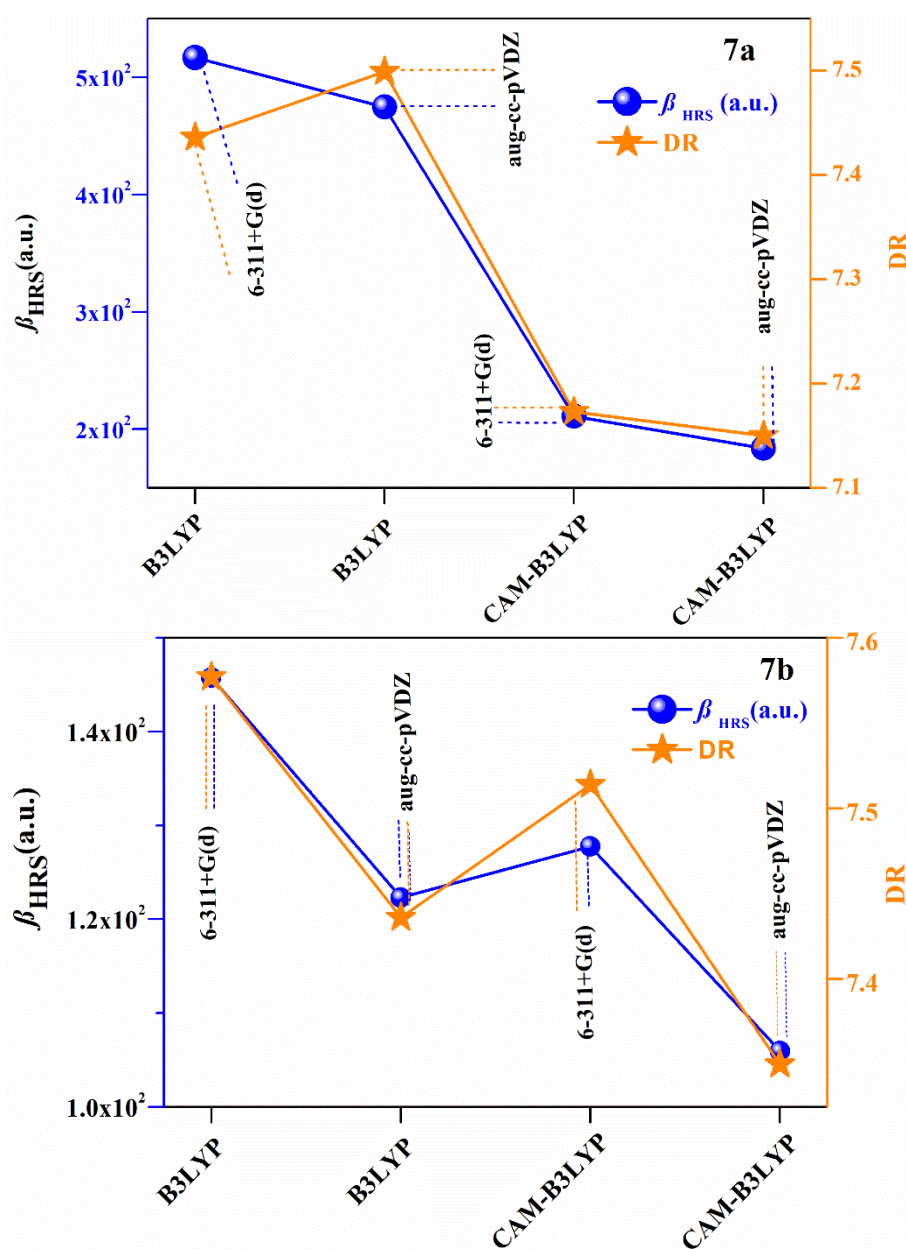


Figure 11. β_{HRS} and DR for bisImCl (**7a**) and bisImPF₆ (**7b**) obtained at different levels theory.

3.8. Frontier molecular orbitals (FMOs)

The energy difference ($\Delta\epsilon$) between the HOMO and LUMO orbitals of these DILs can explain the eventual charge transfer interaction taking place between the cation and anion. The ability to donate an electron is due to the HOMO orbital while the ability to obtain an electron is due to the LUMO. The B3LYP/6-311+G(d) calculations show that $\Delta\epsilon$ varied from

1.96 eV in bisImCl to 3.56 eV in bisImPF₆ (Table 4 and Figure 12), which implies that the bisImCl has low $\Delta\epsilon$ values to transfer electrons between the occupied and unoccupied orbitals.

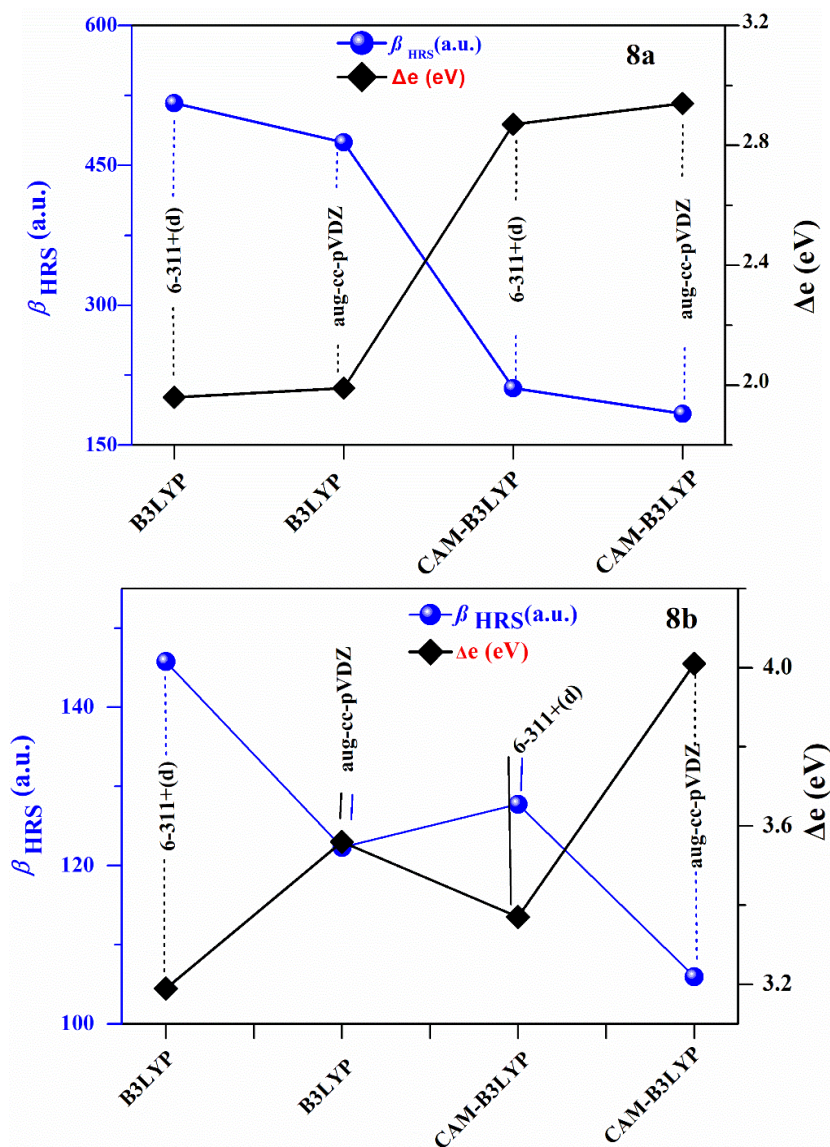


Figure 12. Evolution of the β_{HRS} and $\Delta\epsilon$ for bisImCl (upper panel) and bisImPF₆ (lower panel) determined at different levels of approximation.

Figure 13 shows that the isodensity surface of the HOMO orbital of these two ILs predicted by the two functionals B3LYP and CAM-B3LYP with the two basis sets 6-311+G(d) and aug-cc-pVDZ are similar. The two DFT levels show that these FMOs are π -orbitals originated from p atomic orbitals. The HOMO orbital for the bisImCl is centred in the Cl⁻ anion, while the LUMO orbital is delocalized in the imidazolium ring. This segment shows the positive charge density. In the case of bisImPF₆, the HOMO orbital is delocalised in the imidazolium ring. Unlike bisImCl DIL, the CAM-B3LYP functional using the two

basis sets 6-311+G(d) and aug-cc-pVDZ shows that the HOMO in bisImPF₆ is mainly localized on the phenyl moiety and not in the anion. This fact suggests a weak charge transfer and therefore low hyperpolarizabilities values compared to those obtained for the bisImCl(**Table 4**). The LUMO shows an electron density delocalized over the cation group. In present work, HOMO orbital of bisImPF₆ is delocalised in the imidazolium ring segment and not in the PF₆. Supported by previously reported work [69].

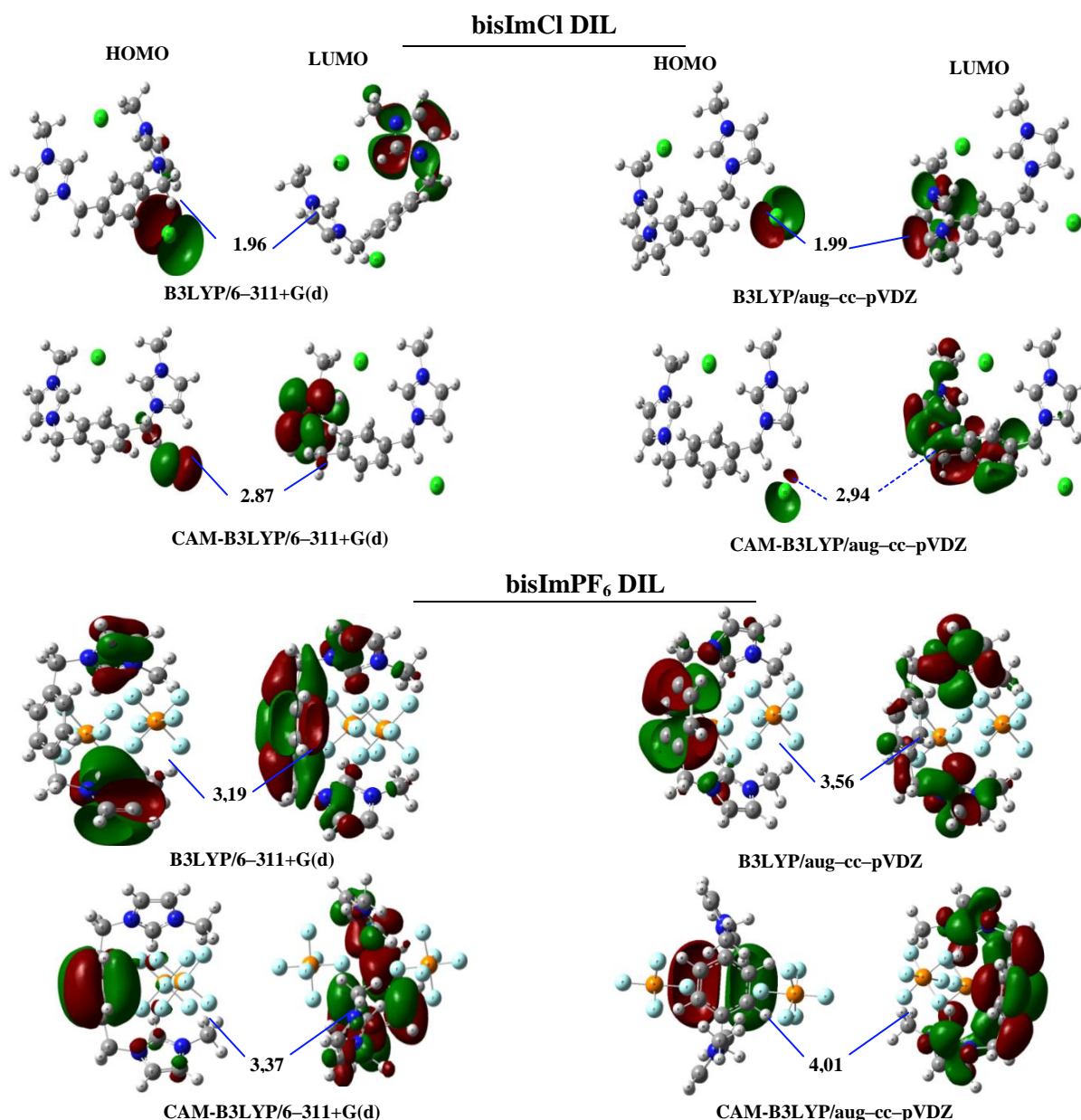


Figure 13. HOMO and LUMO orbitals of bisImCl and bisImPF₆ DIL and their $\Delta\epsilon$ (in eV) estimated by B3LYP and CAM-B3LYP functionals at 6-311+G(d) and aug-cc-pVDZ basis sets.

From these analyses, it can be said that it is reasonable to assume that the imidazolium ring in the case of the bisImPF₆ DIL acts as the main site to donate electrons.

For the bisImCl DIL using the B3LYP/6-311+G(d) calculation, the $\Delta\epsilon$ is 1.96 eV as shown in **Figure 12** and **Table 4**. On the other hand, for the bisImPF₆ DIL, the $\Delta\epsilon$ value was 3.19 eV, which is higher than in bisImCl DIL. The high polarizability and first hyperpolarizability

results for the bisImCl indicate that the bisImCl is easier to polarize, whereas, the bisImPF₆ carries a good resistance for polarization. The high value of gap predicted for bisImPF₆ (3.19 eV) as compared to value obtained for bisImCl (1.96 eV) suggest a high reactivity of bisImCl. Here, the ten H bonds interactions predicted for BisImPF₆ together with the thirteen new RCPs by AIM calculations justify clearly the low reactivity of this ionic liquid.

An inverse relationship has been found between the gaps and β_{HRS} . Indeed, high values of first hyperpolarizabilities β_{HRS} were obtained for low $\Delta\varepsilon$ values. The same observation has been reported in our recent study on the hyperpolarizabilities of the diphenylferrocenylbutene derivatives using theoretical calculations [70].

4. Conclusions

In the present work, two new di-cationic ionic liquids, namely 3,3'-dimethyl-1,1'-(1,4-phenylenedimethylene)-bis(1H-imidazolium) dichloride (bisImCl) and 3,3'-dimethyl-1,1'-(1,4-phenylenedimethylene)-bis(1H-imidazolium) bis(hexafluorophosphate) (bisImPF₆) were successfully synthesized. Both ionic liquids have been characterized by FT-Raman and ¹H- and ¹³C-NMR spectroscopies. Monodentate coordinations of Cl atoms with C-H bonds of imidazolium groups were predicted for BisImCl by B3LYP/6-311++G** calculations while in BisImPF₆ only a PF₆ group is in monodentate coordination with the C-H bond corresponding to cation.

The thermal behavior confirmed that bisImCl and bisImPF₆ have shown good thermal stability. The p-xylyl group plays important role on intermolecular interaction among cation-anion and cation-cation pair. The decomposition temperature of bisImCl is lower than bisImPF₆ DIL. From experimental results, it is clear that the anion can affect significantly on decomposition of these DILs. From Raman vibrational spectra of these DILs, the imidazolium ring vibration modes (C₄-H/C₅-H and C₂-H) are significantly altered depending on nature of anion. The chemical shift of C₂-H proton is more downfield for bisImCl compared to bisImPF₆ DIL. The chemical shifts were strongly influenced in the case of chloride anion and their local environment. Further, higher polarizability (α) and the static first hyperpolarizabilities (β) of these ILs are observed from DFT calculation using different functionals to understand origin of NLO properties. BisImCl has shown higher polarizability (α) and the static first hyperpolarizabilities (β) compared to bisImPF₆. The β values for bisImPF₆ using B3LYP/aug-cc-pVDZ level are more than 5 times of that of urea and bisImCl. However, depolarization ratios (DR) remain constant for these DILs. It is also observed an inversed correlation between the predicted β value and the HOMO-LUMO energy difference ($\Delta\epsilon$) from two state models. The AIM calculations suggest a high stability of bisImPF₆, as compared to bisImCl DIL which is supported by the high gap value predicted for this ionic liquid. Hence, a higher reactivity is revealed for bisImCl DIL.

The complete assignments for cation, bisImCl and bisImPF are here reported together with a set of harmonic scaled force constants calculated for cation and bisImCl.

Acknowledgments

This work was supported by the WBI-COP22 Morocco project and UM5R as well as grants from CIUNT Project N° 26/D608 (Consejo de Investigaciones, Universidad Nacional de Tucumán). The authors would like to thank Prof. Tom Sundius for his permission to use MOLVIB.

ORCID Haddad Boumediene  <https://orcid.org/0000-0001-9198-9528>

ORCID HadjiDjebbar  <http://orcid.org/0000-0003-3058-0627>

ORCID Silvia Antonia Brandán  <https://orcid.org/0000-0003-3604-7743>

ORCID Sumit Kumar Panja <https://orcid.org/0000-0001-5658-0452>

ORCID Annalisa Paolone  <https://orcid.org/0000-0002-4839-7815>

ORCID Mokhtar Draï  <https://orcid.org/0000-0001-5421-5240>

ORCID Didier Villemin  <https://orcid.org/0000-0002-6266-3817>

ORCID Serge Bresson  <https://orcid.org/0000-0003-0932-0468>

ORCID Mustapha Rahmouni  <https://orcid.org/0000-0003-1552-7465>

Compliance with ethical standards

Conflict of interest : The authors declare that they have no conflicts of interest

References

1. R.D. Rogers, K.R. Seddon, Ionic liquids--solvents of the future?, *Science*, 302(5646), (2003) 792-793.
2. E. Sundstrom, J. Yaegashi, J. Yan, F. Masson, G. Papa, A. Rodriguez, ..., J. Gladde., Demonstrating a separation-free process coupling ionic liquid pretreatment, saccharification, and fermentation with *Rhodospiridium toruloides* to produce advanced biofuels, *Green Chem.* 20 (2018) 2870-2879.
3. D.G. Seo, H.C. Moon, Mechanically robust, highly ionic conductive gels based on random copolymers for bending durable electrochemical devices, *Adv. Funct. Mater.* 28 (2018) 1706948.
4. A.A. Elgharbawy, F.A. Riyadi, M.Z. Alam, M. Moniruzzaman, Ionic liquids as a potential solvent for lipase-catalysed reactions: a review, *J. Mol. Liq.* 251 (2018) 150-166.
5. T. Welton, Ionic liquids: a brief history. *Biophysical reviews*, 10 (2018) 691-706.
6. K. Oster, J. Jacquemin, C. Hardacre, A.P.C. Ribeiro, A. Elsinawi, Further development of the predictive models for physical properties of pure ionic liquids: Thermal conductivity and heat capacity, *J. Chem. Thermodyn.*, 118 (2018) 1-15.
7. M.F. Ali, J. Gan, X. Chen, G. Yu, Y. Zhang, M. Ellahi, A.A. Abdeltawab, Hydrodynamic modeling of ionic liquids and conventional amine solvents in bubble column, *Chem. Eng. Res. Des.* 129 (2018) 356-375.
8. J.L. Shamshina, O. Zavgorodnya, P. Berton, P.K. Chhotaray, H. Choudhary, R.D. Rogers, Ionic Liquid Platform for Spinning Composite Chitin–Poly (lactic acid) Fibers, *ACS Sustain. Chem. Eng.* 6 (2018) 10241-10251.
9. M.B. Vazquez-Santos, P. Tartaj, E. Morales, J.M. Amarilla, TiO₂ Nanostructures as Anode Materials for Li/Na-Ion Batteries, *Chem. Rec.* 18 (2018) 1178-1191.
10. B. Haddad, D. Villemin, E.H. Belarbi, N. Bar, M. Rahmouni, New dicationic piperidinium hexafluorophosphate ILs, synthesis, characterization and dielectric measurements, *Arab. J. Chem.* 7 (2014) 781-787.
11. B. Haddad, T. Moumene, D. Villemin, J.F. Lohier, E.H. Belarbi, Bis-methyl imidazolium methylidenebis (trifluoromethanesulfonyl) imide, crystal structure, thermal and dielectric studies, *Bull. Mater. Sci.* 39 (2016) 797-801.
12. D.K. Kaczmarek, K. Czerniak, T. Klejdysz, Dicationic ionic liquids as new feeding deterrents, *Chem. Pap.* 72 (2018) 2457-2466.
13. R.A. Patil, M. Talebi, A. Berthod, D.W. Armstrong, Dicationic ionic liquid thermal decomposition pathways, *Anal. Bioanal. Chem.* 410 (2018) 4645-4655.
14. E. Gurung, D. Meng, L. Xue, G. Tamas, R.M. Lynden-Bell, E.L. Quitevis, Optical Kerr effect spectroscopy of CS₂ in monocationic and dicationic ionic liquids: insights into the intermolecular interactions in ionic liquids, *Phys. Chem. Chem. Phys.* 20 (2018) 26558-26569.
15. J.C. Águila, M. Trejo-Durán, Theoretical study of the second-order nonlinear optical properties of ionic liquids, *J. Mol. Liq.* 269 (2018) 833-838.
16. J.E. Castellanos-Águila, M.A. Olea-Amezcuá, H. Hernández-Cocoletzi, M. Trejo-Durán, Tuning the nonlinear optical properties of the [alkyl-Py]⁺[NO₃]⁻ and [alkyl-MIM]⁺[NO₃]⁻ ionic liquids, *J. Mol. Liq.* 285 (2019) 803-810.
17. I. Severiano-Carrillo, E. Alvarado-Méndez, K.A. Barrera-Rivera, M.A. Vázquez, M. Ortiz-Gutierrez, M. Trejo-Durán, Studies of optical nonlinear properties of asymmetric ionic liquids, *Opt. Mater.* 84 (2018) 166-171.
18. M. Trejo-Durán, E. Alvarado-Méndez, K.A. Barrera-Rivera, V.M. Castaño, Nonlinear optical phenomena in Bi-ionic Liquids, *Optik*, 130 (2017) 895-899.
19. S. Anandhi, K.M. Rahulan, T.S. Shyju, Hyperpolarizability and two photon observation of imidazolium picrate, *Optik*, 125 (2014) 7132-7135.

20. D.J. Williams, Nonlinear optical properties of organic and polymeric materials. In ACS symposium series 233. ACS, (1983).
21. R.F. Souza, M.A.R.C. Alencar, M.R. Meneghetti, J. Dupont, J.M. Hickmann, Nonlocal optical nonlinearity of ionic liquids, *J. Phys. Condens. Matter.* 20 (2008) 155102.
22. M.S. Kodikara, R. Stranger, M.G. Humphrey, Computational studies of the nonlinear optical properties of organometallic complexes, *Coord. Chem. Rev.* 375 (2018) 389-409.
23. G. Marino, P. Segovia, A.V. Krasavin, P. Ginzburg, N. Olivier, G.A. Wurtz, A.V. Zayats, Second-harmonic generation from hyperbolic plasmonic nanorod metamaterials, *Laser Photonics Rev.* 12 (2018) 1700189.
24. O. Ostroverkhova, W.E. Moerner, Organic photorefractives: mechanisms, materials, and applications, *Chem. Rev.* 104 (2004) 3267-3314.
25. C.E. Song, Enantioselective chemo- and bio-catalysis in ionic liquids, *Chem. Comm.* (2004) 1033-1043.
26. S. Bugaychuk, G. Klimusheva, Y. Garbovskiy, T. Mirnaya, A. Ischenko, Nonlinear optical properties of composites based on conductive metal-alkanoate liquid crystals, *Opto-Electron Rev.* 14 (2006) 275-279.
27. B. Haddad, A. Paolone, M. Drai, M. Boumediene, D. Villemin, E.H. Belarbi, ... O. Abbas, Para-xylyl linked bis-imidazolium ionic liquids: A study of the conformers of the cation and of the anion-cation hydrogen bonding, *J. Mol. Struct.*, 1175 (2019) 175-184.
28. R. Bader, AIMPAC: a suite of programs for the theory of atoms in molecules, Hamilton, Canada (contact <http://www.chemistry.mcmaster.ca/aimpac>) Search PubMed; RFW Bader, *Atoms in Molecules: A Quantum Theory*. ISBN: 0198558651, (1990).
29. F.B. König, J. Schönbohm, D. Bayles, AIM2000-a program to analyze and visualize atoms in molecules, *J. Comput. Chem.* 22 (2001) 545-559.
30. P. Pulay, G. Fogarasi, G. Pongor, J.E. Boggs, A. Vargha, Combination of theoretical ab initio and experimental information to obtain reliable harmonic force constants. Scaled quantum mechanical (QM) force fields for glyoxal, acrolein, butadiene, formaldehyde, and ethylene, *J. Am. Chem. Soc.* 105 (1983) 7037-7047.
31. G. Rauhut, P. Pulay, Transferable scaling factors for density functional derived vibrational force fields, *J. Phys. Chem.* 99 (1995) 3093-3100.
32. A.T. Sundius, Scaling of ab initio force fields by MOLVIB, *Vib. Spectrosc.* 29 (2002) 89-95.
33. M.J. Frisch, G.W. Trucks, H.B. Schlegel, G.E. Scuseria, M.A. Robb, J.R. Cheeseman, ... H. Nakatsuji, Gaussian09, revisions D. 01 and B. 01; Gaussian, Inc. Wallingford, CT, (2010).
34. R. Dennington, T. Keith, J. Millam, Semichem Inc., Shawnee Mission Ks. GaussView, Version, 5. (2009).
35. A.D. Becke, Density-functional exchange-energy approximation with correct asymptotic behaviour, *Phy. Rev. A*, 38 (1988) 3098.
36. P. Ugliengo, Moldraw Program. University of Torino, Dipartimento Chimica IFM, Torino, Italy, (1998).
37. H. Boumediene, S.A. Brandán, A.M. Amin, A. Paolone, D. Villemin, S. Bresson, Bidentate cation-anion coordination in the ionic liquid 1-ethyl-3-methylimidazolium hexafluorophosphate supported by vibrational spectra and NBO, AIM and SQMFF calculations, *J. Mol. Struct.* 1212 (2020) 128104.
38. K. Noack, P.S. Schulz, N. Paape, J. Kiefer, P. Wasserscheid, A. Leipertz, The role of the C2 position in interionic interactions of imidazolium based ionic liquids: a vibrational and NMR spectroscopic study, *Phys. Chem. Chem. Phys.* 12 (2010) 14153-14161.

39. A.D. Headley, N.M. Jackson, The effect of the anion on the chemical shifts of the aromatic hydrogen atoms of liquid 1-butyl-3-methylimidazolium salts, *J. Phys. Org.* 15 (2002) 52-55.
40. J. Rigby, E.I. Izgorodina, Assessment of atomic partial charge schemes for polarisation and charge transfer effects in ionic liquids, *Phys. Chem. Chem. Phys.* 15 (2013) 1632-1646.
41. R.K. Blundell, P. Licence, Tuning cation–anion interactions in ionic liquids by changing the conformational flexibility of the cation, *Chem. Commun.* 50 (2014) 12080-12083.
42. P.A. Hunt, I.R. Gould, B. Kirchner, The structure of imidazolium-based ionic liquids: Insights from ion-pair interactions, *Aust. J. Chem.* 60 (2007) 9-14.
43. S. Tsuzuki, H. Tokuda, M. Mikami, Theoretical analysis of the hydrogen bond of imidazolium C 2–H with anions, *Phys. Chem.* 9 (2007) 4780-4784.
44. T. Cremer, C. Kolbeck, K.R. Lovelock, N. Paape, R. Wölfel, P.S. Schulz,... F. Maier, Towards a Molecular Understanding of Cation–Anion Interactions—Probing the Electronic Structure of Imidazolium Ionic Liquids by NMR Spectroscopy, X-ray Photoelectron Spectroscopy and Theoretical Calculations, *Chem. Eur. J.* 16 (2010) 9018-9033.
45. H. Ibrahim, N.A. Koorbanally, D. Ramjugernath, M.D. Bala, V.O. Nyamori, Synthesis and characterization of imidazolium salts bearing fluorinated anions, *Z. Anorg. Allg. Chem.* 638 (2012) 2304-2309.
46. B. Haddad, D. Mokhtar, M. Goussem, E.H. Belarbi, D. Villemin, S. Bresson, ... J. Kiefer, Influence of methyl and propyl groups on the vibrational spectra of two imidazolium ionic liquids and their non-ionic precursors, *J. Mol. Struct.* 1134 (2017) 582-590.
47. B. Haddad, A. Paolone, D. Villemin, J.F. Lohier, M. Draï, S. Bresson,... E.H. Belarbi, para-Xylyl bis-1-methylimidazolium bis (trifluoromethanesulfonyl) imide: Synthesis, crystal structure, thermal stability, vibrational studies, *J. Mol. Liq.* 260 (2018) 391-402.
48. B. Haddad, A. Paolone, D. Villemin, M. Taqiyeddine, E.H. Belarbi, S. Bresson, ... J. Kiefer, Synthesis, conductivity, and vibrational spectroscopy of tetraphenylphosphonium bis (trifluoromethanesulfonyl) imide, *J. Mol. Struct.* 1146 (2017) 203-212.
49. M. Boumediene, B. Haddad, A. Paolone, M. Draï, D. Villemin, M. Rahmouni,... O. Abbas, Synthesis, thermal stability, vibrational spectra and conformational studies of novel dicationic meta-xylyl linked bis-1-methylimidazolium ionic liquids, *J. Mol. Struct.* 1186 (2019) 68-79.
50. A.M. Moschovi, S. Ntais, V. Dracopoulos, V. Nikolakis, Vibrational spectroscopic study of the protic ionic liquid 1-H-3-methylimidazolium bis (trifluoromethanesulfonyl) imide, *Vib. Spectrosc.* 63(2012) 350-359.
51. V.H. Paschoal, L.F. Faria, M.C. Ribeiro, Vibrational Spectroscopy of Ionic Liquids, *Chem. Rev.* 117 (2017) 7053-7112.
52. T. Endo, H. Murata, M. Imanari, N. Mizushima, H. Seki, K. Nishikawa, NMR Study of Cation Dynamics in Three Crystalline States of 1-Butyl-3-methylimidazolium Hexafluorophosphate Exhibiting Crystal Polymorphism, *J. Phys. Chem. B*, 116 (2012) 3780–3788.
53. E.R. Talaty, S. Raja, V.J. Storhaug, A. Dölle, W.R. Carper, Raman and infrared spectra and ab initio calculations of C2-4MIM imidazolium hexafluorophosphate ionic liquids, *J. Phys. Chem. B*, 108 (2004) 13177-13184.
54. B. Haddad, J. Kiefer, H. Brahim, E.-h. Belarbi, D. Villemin, S. Bresson, O. Abbas, M. Rahmouni, A. Paolone, O. Palumbo, Effects of C(2) Methylation on Thermal Behavior and Interionic Interactions in Imidazolium-Based Ionic Liquids with Highly Symmetric Anions, *Appl. Sci.* 8 (7) (2018) 1043.

55. T. Moumene, E.H. Belarbi, B. Haddad, D. Villemin, O. Abbas, B. Khelifa, S. Bresson, Vibrational Spectroscopic Study of Imidazolium Dicationic Ionic Liquids: Effect of Cation Alkyl Chain Length, *J. Appl. Spectrosc.* 83 (2) (2016)165-171.
56. F. Castet, E. Bogdan, A. Plaquet, L. Ducasse, B. Champagne, V. Rodriguez, Reference molecules for nonlinear optics: A joint experimental and theoretical investigation,*J. Chem. Phys.* 136 (2012) 024506.
57. R. Bersohn, Y.H. Pao, H.L. Frisch, Double-quantum light scattering by molecules,*J. Chem. Phys.* 45 (1966) 3184-3198.
58. V. Rodriguez, J. Grondin, F. Adamietz, Y. Danten, Local structure in ionic liquids investigated by hyper-Rayleigh scattering,*J Phys. Chem. B*, 114 (2010) 15057-15065.
59. D. Hadji, A. Rahmouni, Theoretical study of nonlinear optical properties of some azoic dyes, *Mediterr. J. Chem.*, 4 (2015) 185-192.
60. D. Hadji, A. Rahmouni, Molecular structure, linear and nonlinear optical properties of some cyclic phosphazenes: A theoretical investigation,*J. Mol. Struct.* 1106 (2016) 343-351.
61. D. Hadji, H. Brahim, Structural, optical and nonlinear optical properties and TD-DFT analysis of heteroleptic bis-cyclometalated iridium (III) complex containing 2-phenylpyridine and picolinate ligands,*Theor. Chem. Acc.* 137 (2018) 180.
62. M. Shkir, S. AlFaify, H. Abbas, S. Muhammad, First principal studies of spectroscopic (IR and Raman, UV–visible), molecular structure, linear and nonlinear optical properties of l-arginine p-nitrobenzoate monohydrate (LANB): a new non-centrosymmetric material. *Spectrochimica Acta Part A*, 147 (2015) 84-92.
63. G. Raabe, J. Köhler, Thermodynamical and structural properties of imidazolium based ionic liquids from molecular simulation,*J. Chem. Phys.* 128 (2008) 154509
64. D.M. Bishop, J. Pipin, Dipole, quadrupole, octupole, and dipole–octupole polarizabilities at real and imaginary frequencies for H, HE, and H₂ and the dispersion-energy coefficients for interactions between them,*Int. J. Quantum Chem.* 45 (1993) 349-361.
65. I. Khan, M. Taha, P. Ribeiro-Claro, S.P. Pinho, J.A. Coutinho, Effect of the cation on the interactions between alkyl methyl imidazolium chloride ionic liquids and water,*J. Chem. Phys. B*, 118 (2014) 10503-10514.
66. Z.H. Zhang, J.S. Li, J. Tang, L.L. Yang, K.X. Guo, J.H. Yuan, Binding energy and the third-order nonlinear optical susceptibility of an exciton in GaAs/AlGaAs core/shell spherical quantum dot,*J. Opt.* 47 (2018) 445-455.
67. D. Sakthi, M. Prakasam, A. Prakasam, S. Sivakumar, P.M. Anbarasan, A Complete DFT, TD-DFT and Non-Linear Optical Property Study on 6-Amino-2-Methylpyridine-3-Carbonitrile, *Computational Chemistry*, 5 (2017) 129.
68. I. Ledoux, J. Zyss, Influence of the molecular environment in solution measurements of the second-order optical susceptibility for urea and derivatives,*Chem. Phys.* 73 (1982) 203-213.
69. A. Yousefi, S. Javadian, N. Dalir, J. Kakemam, J. Akbari, Imidazolium-based ionic liquids as modulators of corrosion inhibition of SDS on mild steel in hydrochloric acid solutions: experimental and theoretical studies, *RSC Advances*, 5 (2015) 11697-11713.
70. D. Hadji, A. Rahmouni, D. Hammoutène, O. Zekri, First theoretical study of linear and nonlinear optical properties of diphenyl ferrocenyl butene derivatives, *J.Mol. Liq.* 286 (2019) 110939.

